Molecular Orbital Study of Zinc(II)-Catalyzed Alternating Copolymerization of Carbon Dioxide with Epoxide

Zhiwei Liu,† Maricel Torrent, and Keiji Morokuma*

Cherry L. Emerson Center for Scientific Computation and Department of Chemistry, Emory University, Atlanta, Georgia 30322

Received December 20, 2001

The mechanism of copolymerization of CO_2 with cyclohexene oxide catalyzed by the Zn(II) organometallic compound (BDI)ZnOCH$_3$ (BDI = N(2,6-^{i}Pr$_2$C$_6$H$_3$)C(Me)CHC(Me)N(2,6-^{i}Pr$_2$C$_6$H$_3$) chelating β-diimine ligand) has been studied with the hybrid molecular orbital (MO) method ONIOM, combining the density functional method B3LYP/LANL2DZ(d) with the semiempirical MO method PM3. In particular, the insertions of CO_2 and cyclohexene oxide/ethylene oxide into zinc−alkoxyl and zinc−carbonate bonds have been investigated in detail. The insertion of CO_2 into either a zinc−alkoxyl (epoxide + CO_2 alternating insertion) or zinc−carbonate (consecutive CO_2 insertion) bond has been found to be thermodynamically less favorable but is in general kinetically favored over the insertion of epoxide, due to a high barrier for the latter. This high barrier is associated with a rather asynchronous transition state where the ring opening has taken place and yet the C−O bond is not formed. However, only in the case of insertion of sterically strained cyclohexene oxide into the zinc−carbonate bond is the barrier low enough to compete with CO_2 insertion, resulting in alternating copolymerization. This lowering is driven by the release of the extra strain energy in the three- and six-membered-ring bicyclic structure in cyclohexene oxide. The rate-determining step in copolymerization is epoxide insertion, which can be controlled by the catalyst and the epoxide.

I. Introduction

Although carbon dioxide (CO_2) is naturally abundant, relatively nontoxic, and inexpensive and is one of the major ingredients in carbon management,[1] synthetic processes utilizing this attractive raw material have hardly been successfully exploited. One of the more flourishing processes of CO_2 utilization is the formation of polycarbonate by copolymerization of CO_2 with epoxide. Recently, the search for more efficient catalysts for CO_2/epoxide copolymerization has received considerable attention. A variety of active catalysts, from simple alkali-metal salts to classical organometallic complexes, for CO_2/epoxide copolymerization has been thoroughly reviewed by Darensbourg and Holtcamp.[2] The Zn(II)-based catalysts reported by Darensbourg,[3] Beckman,[4] and Coates[5,6] are among those that are highly active for copolymerization of CO_2 and epoxide. However, as pointed out by Darensbourg and Holtcamp, there appears to be a lack of information on the detailed catalytic mechanism. Here we present the first theoretical study on the Zn(II)-catalyzed alternating copolymerization reaction of CO_2 with epoxide for Zn(II) complexes with the chelating bulky β-diimine ligands from Coates' work, represented by (BDI)ZnX, where BDI is the N(2,6-^{i}Pr$_2$C$_6$H$_3$)C(Me)CHC(Me)N(2,6-^{i}Pr$_2$C$_6$H$_3$) chelating ligand and X = OC(CH$_3$)O (**1**), OCH$_3$ (**2**). The choice of the catalysts studied is based on the fact that these are the most active among all reported Zn-based catalysts. The purpose of the present study is to shed some light on the catalytic reaction mechanism of the title process.

Coates et al. have recently proposed that the copolymerization reaction proceeds as insertion of CO_2 into a metal−alkoxyl bond followed by ring opening and insertion of epoxide into a metal−carbonate bond and repetition of these alternating insertion processes.[5] In our theoretical study we will determine the structures and energies of intermediates and transition states (TSs) on the desired alternating insertion pathways and

† Present address: Rohm and Haas Co., Spring House Technical Center, P.O. Box 904, Spring House, PA 19477-0904.

(1) Arakawa, H.; Aresta, M.; Armor, J. N.; Barteau, M. A.; Beckman, E. J.; Bell, A. T.; Bercaw, J. E.; Creutz, C.; Dinjus, E.; Dixon, D. A.; Domen, K.; DuBois, D. L.; Eckert, J.; Fujita, E.; Gibson, D. H.; Goddard, W. A.; Goodman, D. W.; Keller, J.; Kubas, G. J.; Kung, H. H.; Lyons, J. E.; Manzer, L. E.; Marks, T. J.; Morokuma, K.; Nicholas, K. M.; Periana, R.; Que, L.; Rostrup-Nielson, J.; Sachtler, W. M. H.; Schmidt, L. D.; Sen, A.; Somorjai, G. A.; Stair, P. C.; Stults, B. R.; Tumas, W. *Chem. Rev.* **2001**, *101*, 953−996.

(2) Darensbourg, D. J.; Holtcamp, M. W. *Coord. Chem. Rev.* **1996**, *153*, 155−174.

(3) Darensbourg, D. J.; Holtcamp, M. W. *Macromolecules* **1995**, *28*, 7577−7579.

(4) (a) Super, M. S.; Berluche, E.; Costello, C.; Beckman, E. J. *Macromolecules* **1997**, *30*, 368. (b) Super, M. S.; Beckman, E. J. *Macromol. Symp.* **1998**, *127*, 89−108.

(5) Cheng, M.; Lobkovsky; E. B.; Coates, G. W. *J. Am. Chem. Soc.* **1998**, *120*, 11018−11019.

(6) Cheng, M.; Darling, N. A.; Lobkovsky; E. B.; Coates, G. W *Chem. Commun.* **2000**, 2007−2008.

10.1021/om0110843 CCC: $22.00
Publication on Web 02/14/2002

Scheme 1 . Suggested Schematic Picture of Insertions A−D as Reaction Pathways for CO_2/Epoxide Copolymerization Catalyzed by (BDI)ZnOCH$_3$

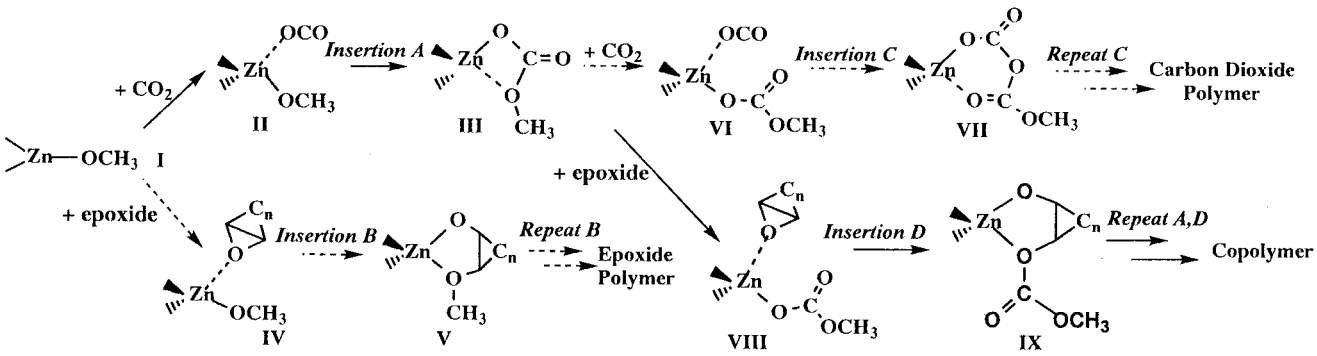

Chart 1. ONIOM Scheme Used in the Present Paper for Complex 1 and Its Dimer $(1)_2$[a]

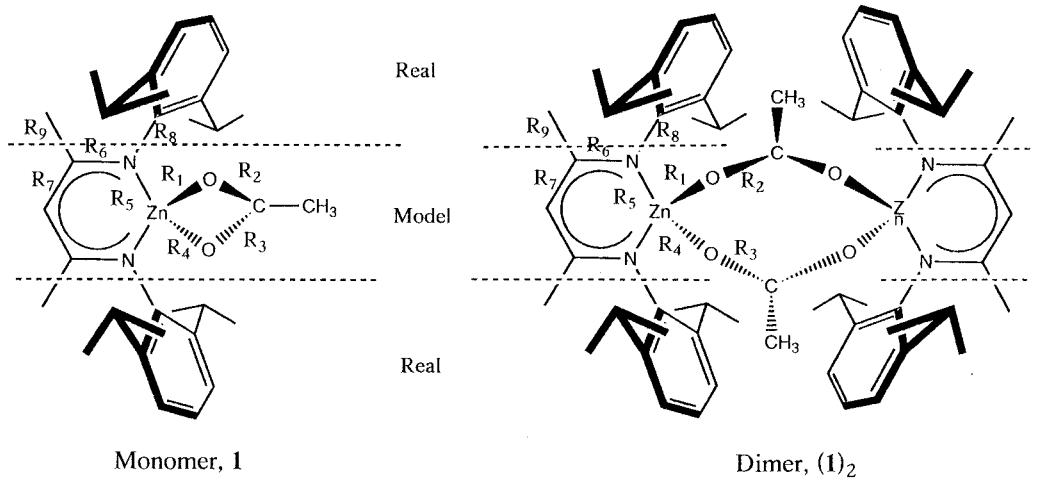

[a] The same scheme was used for the active catalyst (BDI)ZnOCH$_3$ (**I**). The substrates (CO_2, OC_2H_4, OC_6H_{10}) are always included in the model system.

compare them with energies on competing pathways. The schematic reaction pathways are presented in Scheme 1 and

Insertion A: [Zn]-OR + CO_2 → [Zn]-OC(O)-OR

Insertion B: [Zn]-OR +  → [Zn]-OCC-OR

Insertion C: [Zn]-OC(O)OR + CO_2 → [Zn]-OC(O)-OC(O)OR

Insertion D: [Zn]-OC(O)OR +  → [Zn]-OCC-OC(O)OR

As shown above, there are four possible insertion steps: (A) insertion of CO_2 into the metal−alkoxyl bond, (B) insertion of epoxide into the metal−alkoxyl bond, (C) insertion of CO_2 into the metal−carbonate bond, and (D) insertion of epoxide into the metal−carbonate bond. Insertion A followed by insertion D is the perfect alternating reaction pathway, while insertion steps B and C indicate competing pathways destroying alternating copolymerization. In the current study, we have followed the strategy by Svensson et al.[7] in a recent density functional (DFT) study on the alternating copolymerization of carbon monoxide with ethylene. By investigating both the perfect alternating pathway and competing pathways, they have clarified the controlling factors of different mechanisms and provided a reasonable explanation for experimental observations.

The present paper is organized as follows. In section II, we discuss the computational methods used in the current study, as well as calibration calculations that validate the chosen ONIOM scheme. In section III, we discuss the structures and energies of all intermediates and TSs involved in both the alternating and competing pathways. The overall potential energy surfaces (PESs) and the preferred reaction pathways are also summarized therein. Finally, in section IV, we present several conclusions.

II. Computational Details and Calibration Calculations

The active catalyst species we adopted in the present study is the zinc diimine complex studied by Coates experimentally,[5] (BDI)ZnOCH$_3$, where BDI is the N(2,6-^{i}Pr$_2$C$_6$H$_3$)C(Me)CHC(Me)-N(2,6-^{i}Pr$_2$C$_6$H$_3$) chelating ligand, as shown in Chart 1. According to Coates, this compound exists in a monomeric state in tetrahydrofuran-d_8 solution (10^{-2} M) and the dimerization equilibrium constant for K_{eq} is 34 M^{-1} in C_6D_6 solution. As the polymerizing monomers, in addition to carbon dioxide, we used ethylene oxide (C_2H_4O) as well as the experimentally studied cyclohexene oxide ($C_6H_{10}O$). Geometries of all reactants, intermediates, TSs, and products involved in the CO_2/C_2H_4O (or $C_6H_{10}O$) copolymerization by (BDI)ZnOCH$_3$ have been fully optimized with the two-layer ONIOM(B3LYP:PM3) method.

(7) Svensson, M.; Matsubara, T.; Morokuma, K. *Organometallics* **1996**, *15*, 5568−5576.

The two-layer ONIOM method[8−10] generates a smaller "model system" from the "real system" under study, applying a "high level" method to the "model system" and a "low level" method to both the "real system" and "model system" and estimating the results of the "high level" calculation for the "real system" by

$$E(\text{ONIOM,real}) = E(\text{high,model}) + E(\text{low,real}) - E(\text{low,model})$$

In the present study, the "model system" contains, in addition to all substrates (CO_2, C_2H_4O and $C_6H_{10}O$), the truncated chelating ligand (NHCHCHCHNH), replacing four substituents on the β-diimine ligands BDI, two methyl groups, and two 2,6-isopropylphenyl groups by hydrogen atoms, as shown in Scheme 2. The "high level" in the present study is the B3LYP density functional method,[11−13] and the "low level" is the semiempirical PM3[14] method.

Two basis sets, denoted as BS I and BS II, are used with the B3LYP method. BS I is simply the LANL2DZ basis set, which includes (1) Hay−Wadt effective core potentials (ECP) replacing electrons up to 2p and a (8s5p5d)/[3s3p2d] valence basis set for Zn[15,16] and (2) Huzinaga−Dunning valence double-ζ basis sets[17] for all other atoms. BS II is based on BS I augmented with one set of d polarization functions for each C or O atom in the OCH_3, CO_2, and C_2H_4O (or $C_6H_{10}O$) groups.

To identify equilibrium structures and TSs, as well as to evaluate the zero point energy (ZPE) corrections and free energies, frequency calculations were performed on all optimized structures at the ONIOM(B3LYP/BS II:PM3) level of theory. For several selected intermediates and TSs, the full (non-ONIOM) density functional energy calculations at the B3LYP/BS II level have been carried out for the ONIOM optimized structures to evaluate the errors the ONIOM method might introduce on energies. All calculations are performed using the Gaussian98 package.[18]

Furthermore, to clarify the origin of the differences in energetics between cyclohexene oxide and ethylene oxide, we have also carried out calculations on reaction energies of the two catalyst-free ring-opening nucleophilic addition reactions (1) $C_2H_4O + H_2O \rightarrow C_2H_6O_2$ and (2) $C_6H_{10}O + H_2O \rightarrow C_6H_{12}O_2$, at the B3LYP/BS II and G2MS[19] levels of theory. The G2MS method, a variation of the G2 type method, gives excellent energetics within an error of a few kilocalories per mole that can be compared directly with the experimental reaction thermodynamics data from the NIST database and can be used to validate the B3LYP/BS II results.

It should be noted that all the reactions have been performed in neat cyclohexene oxide.[5] This suggests that the solvent effect will be small for the reaction of the neutral catalyst. Therefore, we did not take into account the effects of solvent.

Calibration of the B3LYP/BS I:PM3 Combination in the ONIOM Method. To examine whether the combination of B3LYP/BS I with PM3 in the ONIOM scheme gives reasonable results for the current system, we have carried out a series of geometry optimization on (BDI)ZnAc, Ac═OC(CH$_3$)O (**1**; see Chart 1) and related complexes at different levels of theory. Specifically, compound **1** has been optimized using both B3LYP/BS I (**A**) and ONIOM(B3LYP/BS I:PM3) (**B**) methods, while the simplified model compound **1m** with the truncated ligand (NHCHCHCHNH) has been calculated at the B3LYP/BS I level (**C**). Since the only available experimental structural information is the X-ray structure of the dimer of **1**, **(1)$_2$**, geometry optimizations of the dimer compound, **(1)$_2$**, and the model dimer compound, **(1m)$_2$**, have also been carried out at the ONIOM(B3LYP/BS I:PM3) (**E**) and B3LYP/BS I (**D**) levels of theory, respectively. The optimized structures are shown in Table 1, with the bond labels given in Chart 1. All the structures have tetrahedral Zn centers with two coordinated N atoms from the chelating diimine ligands. The other two sites of the tetrahedron are occupied by two O atoms, which are both from one chelating acetate ligand in compounds **1** and **1m** and from two acetate ligands in the dimers (**1**)$_2$ and (**1m**)$_2$. The N−Zn−N chelate plane is nearly perpendicular to the O−Zn−O plane. In the real systems **1** and (**1**)$_2$ the phenyl plane is nearly perpendicular to the N−Zn−N chelate. The overall structural features are consistent with the experimental X-ray structure of (**1**)$_2$.

Entries **A**−**C** of Table 1 allow us to compare structural data of the ONIOM calculation on the large real system (**B**) or of the B3LYP calculation on the simplified small model system (**C**) to those of the full B3LYP calculation on the large real system (**A**). First of all, the bond lengths in **A**−**C** are all similar to each other, with the maximum difference of 0.06 Å. There are only minor differences (<0.01 Å) in the Zn−O and C−O bond lengths, R_1−R_4, between real and model systems or between B3LYP and ONIOM calculations. For R_5−R_7, the Zn−N, N−C, and C−C distances of **1** (**B**) at the ONIOM level are 0.063, 0.016, and 0.002 Å longer than that of **1** (**A**) at the B3LYP/BS I level. On the other hand, the differences in R_5−R_7 between **1m** (**C**) and **1** (**A**), both calculated at the B3LYP level, are 0.001, −0.008, and 0.008 Å, respectively. Therefore, from full B3LYP calculations on the large real systems (**A**), the ONIOM calculation on the large real system (**B**) deviates more at the Zn−N and N−C bonds but less at the C−C bond than B3LYP on the simplified small model system. Overall, for structural features of the core layer, the B3LYP calculation on **1m** agrees slightly better with the full B3LYP calculation on **1** than the ONIOM calculation on **1**. For the linkage distances R_8 and R_9, differences of 0.03 and −0.03 Å, respectively, are found between the B3LYP (**A**) and ONIOM (**B**) calculations. In the ONIOM scheme, the distances of the linkage bonds X−C (X = C, N) are related with the distance of the corresponding X−H bond by a g factor, $R_{X-H} = gR_{X-C}$. Furthermore, the choice of g factors should have indirect effects on the optimization of Zn−N, N−C, and C−C bonds, which are next to the linkage X−C (X = C, N) bonds. In the present study, default values were used for the g factors; with an optimized choice of g factors, the agreement might be improved for R_5−R_9. In a brief conclusion, the ONIOM calculation on the large real system generates the optimized structure, which is almost as good as the full B3LYP calculation.

Entries **D**−**F** in Table 1 give the calculated bond distances in dimer (**1**)$_2$ or (**1m**)$_2$, as well as the experimental X-ray structural data of (**1**)$_2$. Bond lengths of (**1m**)$_2$ or (**1**)$_2$ that are

(8) Humbel, S.; Sieber, S.; Morokuma, K. *J. Chem. Phys.* **1996**, *105*, 1959−1967.
(9) Svensson, M.; Humbel, S.; Froese, R. D. J.; Matsubara, T.; Sieber, S.; Morokuma, K. *J. Phys. Chem.* **1996**, *100*, 19357−19363.
(10) Dapprich, S.; Komaromi, I.; Byun, K. S.; Morokuma, K.; Frisch, M. J. *J. Mol. Struct. (THEOCHEM)* **1998**, *461*−*462*, 1−21.
(11) Becke, A. D. *Phys. Rev. A* **1988**, *38*, 3098.
(12) Lee, C.; Yang, W.; Parr, R. G. *Phys. Rev. B* **1988**, *37*, 785.
(13) Becke, A. D. *J. Chem. Phys.* **1993**, *98*, 5648.
(14) Stewart, J. J. P. *J. Comput. Chem.* **1989**, *10*, 209.
(15) Hay, P. J.; Wadt, W. R. *J. Chem. Phys.* **1985**, *82*, 299.
(16) Wadt, W. R.; Hay, P. J. *J. Chem. Phys.* **1985**, *82*, 284.
(17) (a) Dunning, T. M., Jr. *J. Chem. Phys.* **1971**, *55*, 716. (b) Dunning, T. M., Jr. *J. Chem. Phys.* **1970**, *53*, 2823.
(18) Frisch, M. J.; Trucks, G. W.; Schlegel, H. B.; Scuseria, G. E.; Robb, M. A.; Cheeseman, J. R.; Zakrzewski, V. G.; Montgomery, J. A., Jr.; Stratmann, R. E.; Burant, J. C.; Dapprich, S.; Millam, J. M.; Daniels, A. D.; Kudin, K. N.; Strain, M. C.; Farkas, O.; Tomasi, J.; Barone, V.; Cossi, M.; Cammi, R.; Mennucci, B.; Pomelli, C.; Adamo, C.; Clifford, S.; Ochterski, J.; Petersson, G. A.; Ayala, P. Y.; Cui, Q.; Morokuma, K.; Malick, D. K.; Rabuck, A. D.; Raghavachari, K.; Foresman, J. B.; Cioslowski, J.; Ortiz, J. V.; Stefanov, B. B.; Liu, G.; Liashenko, A.; Piskorz, P.; Komaromi, I.; Gomperts, R.; Martin, R. L.; Fox, D. J.; Keith, T.; Al-Laham, M. A.; Peng, C. Y.; Nanayakkara, A.; Gonzalez, C.; Challacombe, M.; Gill, P. M. W.; Johnson, B. G.; Chen, W.; Wong, M. W.; Andres, J. L.; Head-Gordon, M.; Replogle, E. S.; Pople, J. A. *Gaussian 98*, revision A.1; Gaussian, Inc.: Pittsburgh, PA, 1998.
(19) Froese, R. D. J.; Humbel, S.; Svensson, M.; Morokuma, K. *J. Phys. Chem. A* **1997**, *101*, 227−233.

Table 1. Comparison of Bond Distances (Labeled in Chart 1; in Å) in Catalyst 1 and Its Model 1m from B3LYP and ONIOM Calculations and Experiment

	system; method	CPU time (h)	R_1	R_2	R_3	R_4	R_5	R_6	R_7	R_8	R_9
A	real **1**; B3LYP/BS I	600	2.126	1.311	1.307	2.138	1.992	1.353	1.421	1.453	1.525
B	real **1**; ONIOM(B3LYP/BS I:PM3)	15	2.121[a]	1.311[a]	1.308[a]	2.132[a]	2.055[a]	1.369[a]	1.423[a]	1.483[b]	1.498[b]
C	model **1m**; B3LYP/BS I		2.124	1.310	1.308	2.133	1.993	1.345	1.413	1.020 (H)	1.095 (H)
D	model dimer $(\mathbf{1m})_2$; B3LYP/BS I		1.997	1.287	1.291	1.995	2.014	1.343	1.413	1.021 (H)	1.096 (H)
E	real dimer $(\mathbf{1})_2$; ONIOM(B3LYP/BS I:PM3)	60	1.989[a]	1.287[a]	1.289[a]	1.990[a]	2.085[a]	1.367[a]	1.424[a]	1.483[b]	1.500[b]
F	real dimer $(\mathbf{1})_2$; X-ray structure		1.965	1.228	1.238	1.945	1.971	1.332	1.391	1.437	1.508

[a] These bond distances determined mainly by the high level, B3LYP. [b] These link-bond distances are determined interdependently by B3LYP and PM3 methods. See text for details.

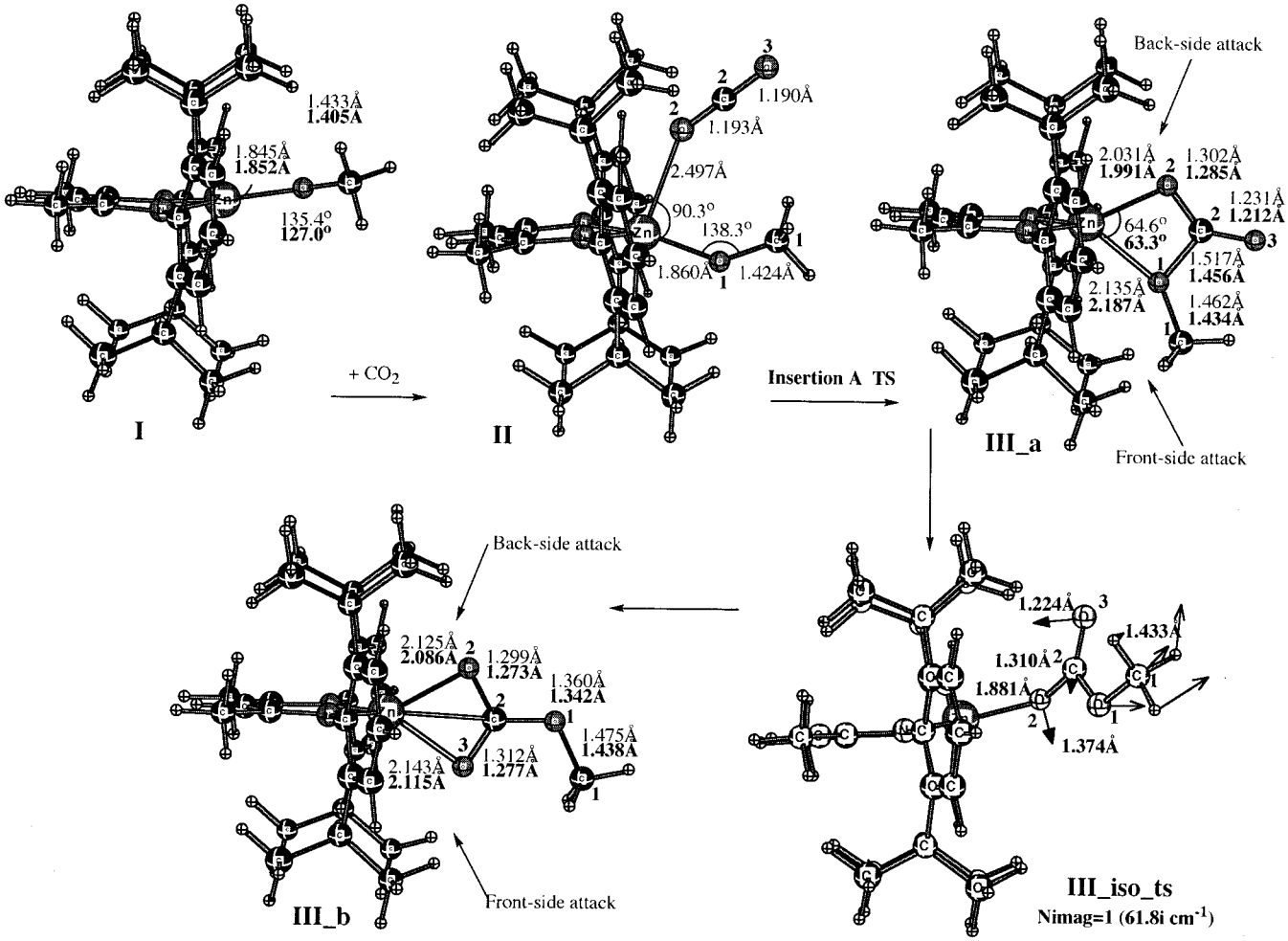

Figure 1. ONIOM(B3LYP:PM3) optimized structures of intermediates and TSs in insertion A of the CO_2/OC_2H_4 copolymerization catalyzed by $(BDI)ZnOCH_3$. Lightface numbers indicate bond lengths and bond angles using BS I and boldface numbers those using BS II.

calculated at either the B3LYP or ONIOM level agree fairly well with the X-ray structural data. Overall, the calculated bond distances are about 0.02−0.04 Å longer than those in the solid state, measured by X-ray crystallography. Two C−O bond lengths, R_2 and R_3, are about 0.05∼0.06 Å larger than the experimental X-ray values. The differences can be reduced if polarization functions are added to the double-ζ basis sets of C and O. As shown in Figures 1−4, this is confirmed by comparing many optimized structures using BS I and BS II, which are without and with polarization functions, respectively. The Zn−N bond length R_5 of 2.085 Å, obtained by ONIOM, is about 0.1 Å larger than that of the experimental value. However, the R_5 value of 2.014 Å in the model dimer $(\mathbf{1m})_2$, calculated by B3LYP (**E**), is in much better agreement with the experiment. The same trends are also observed in the monomer calculations **A**−**C**, in which R_5 values of the real and model systems at B3LYP (**A** and **C**) are almost equal to each other and are about 0.07 Å shorter than that of the real system at ONIOM (**B**). We notice that the Zn−N bond is next to the substitution of *N*-diisopropylphenyl by *N*-H. Therefore, the large discrepancy in R_5 is caused by the choice of the ONIOM scheme or the *g* factor. Since the diimine ligands will not be directly involved in the copolymerization process, we expect the deviation of 0.1 Å for R_5 shall not have a significant effect on the reaction mechanism study. Overall, the results indicate that the ONIOM scheme, combining the density functional method B3LYP and inexpensive semiempirical method PM3, works well in obtaining reliable molecular structures for the Zn(II) catalysts.

The computational advantage of ONIOM over the full B3LYP calculation is overwhelming. As seen in Table 1, for the real complex **1**, the ONIOM(B3LYP/BS I:PM3) calculation

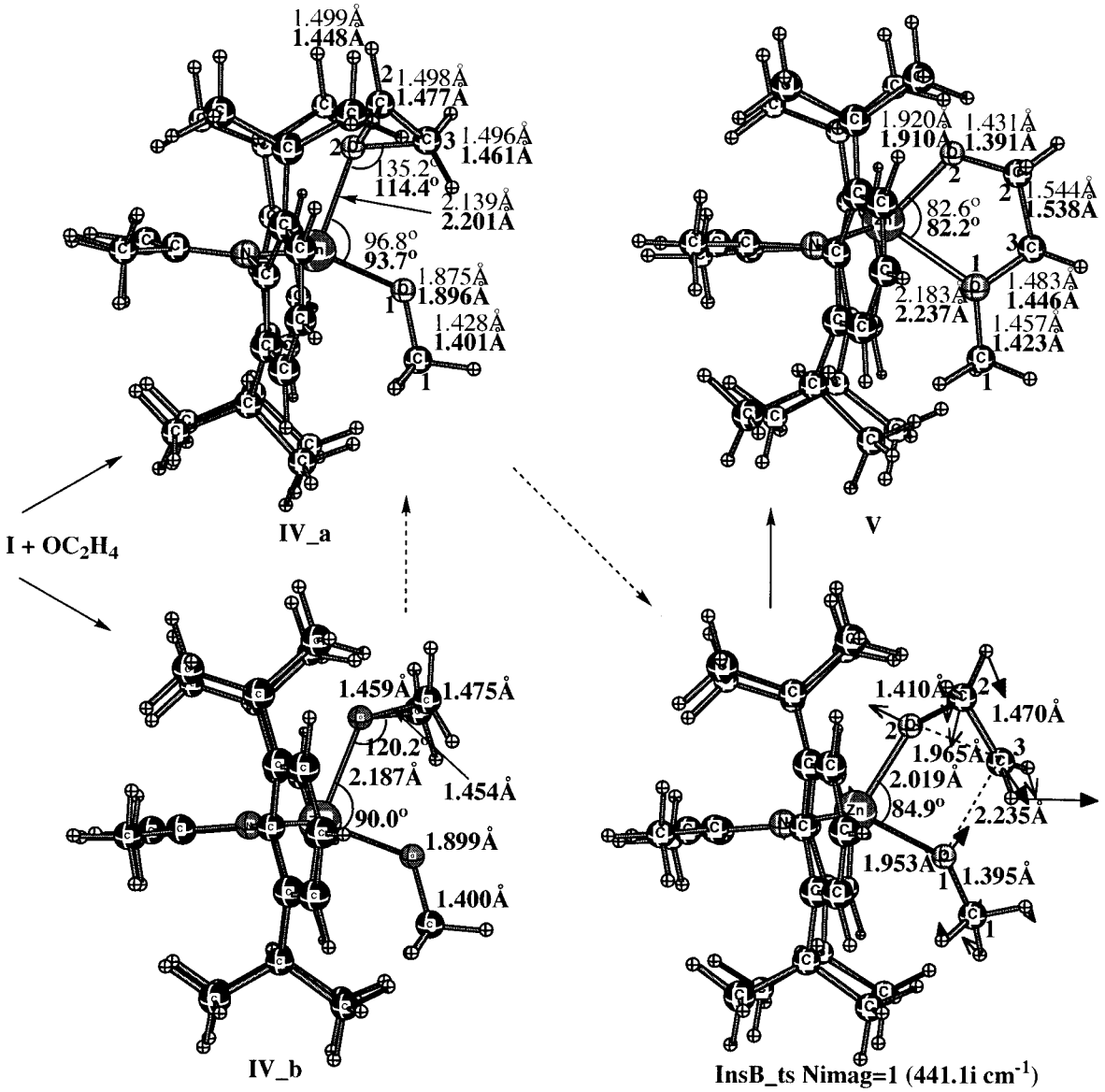

Figure 2. ONIOM(B3LYP:PM3) optimized structures of intermediates and TSs in insertion B of the CO_2/OC_2H_4 copolymerization catalyzed by (BDI)ZnOCH_3. Lightface numbers indicate bond lengths and bond angles using BS I and boldface numbers those using BS II.

is 40 times faster than the full B3LYP/BS I calculation. It is not an exaggeration to say that, without the ONIOM method, the present project would have been impossible.

III. Structures and Energies of Intermediates and Transition States

In this section, we will discuss both energies and geometries obtained mostly from optimizations with the larger basis set, i.e., at the ONIOM(B3LYP/BS II:PM3) level. All intermediates and TSs were optimized without symmetry constraint. Figures 1−4 show the ONIOM-(B3LYP/BS I:PM3) and ONIOM(B3LYP/BS II:M3) optimized structures for all intermediates and TSs of insertions A−D, respectively, of CO_2 and C_2H_4O. In some of the intermediates and TSs, O and C atoms at the active sites are numbered for the convenience of discussion. In the text, we mainly discuss the geometries at the more reliable ONIOM(B3LYP/BS II:PM3) level. The ONIOM(B3LYP/BS II:PM3) optimized structures of selected intermediates and TSs with $C_6H_{10}O$ are shown in Figure 5 (in which the label CHO indicates $C_6H_{10}O$). The ONIOM(B3LYP/BS II:PM3) energies and Gibbs free energies at 298.15 K and 1 atm of all intermediates and TSs, as well as the B3LYP/BS II single-point energies on a few selected complexes and TSs, relative to the reactant **I** + appropriate number of free CO_2, C_2H_4O, or $C_6H_{10}O$ molecules, are given in Table 2.

A. CO_2 Insertion into the Zinc−Alkoxyl Bond. The reactant complex **I** is an unsaturated 16-electron complex. The trigonal coordination of Zn(II) with one oxygen and two nitrogens is nearly coplanar, as shown in Figure 1. The methyl group is nearly in the same plane, with a C−O−Zn angle of 127.0°. The Zn−N bond cis to the methyl group is 0.01 Å longer than the other Zn−N bond. The Zn−O (σ-bond) length is 1.852 Å. No stable CO_2 complex, (BDI)Zn$(CO_2)(OCH_3)$ (**II**), could be located by geometry optimizations using BS II. Our calculations converge to insertion product **III_a**. Using BS I, the very weak complex **II** was obtained, with a

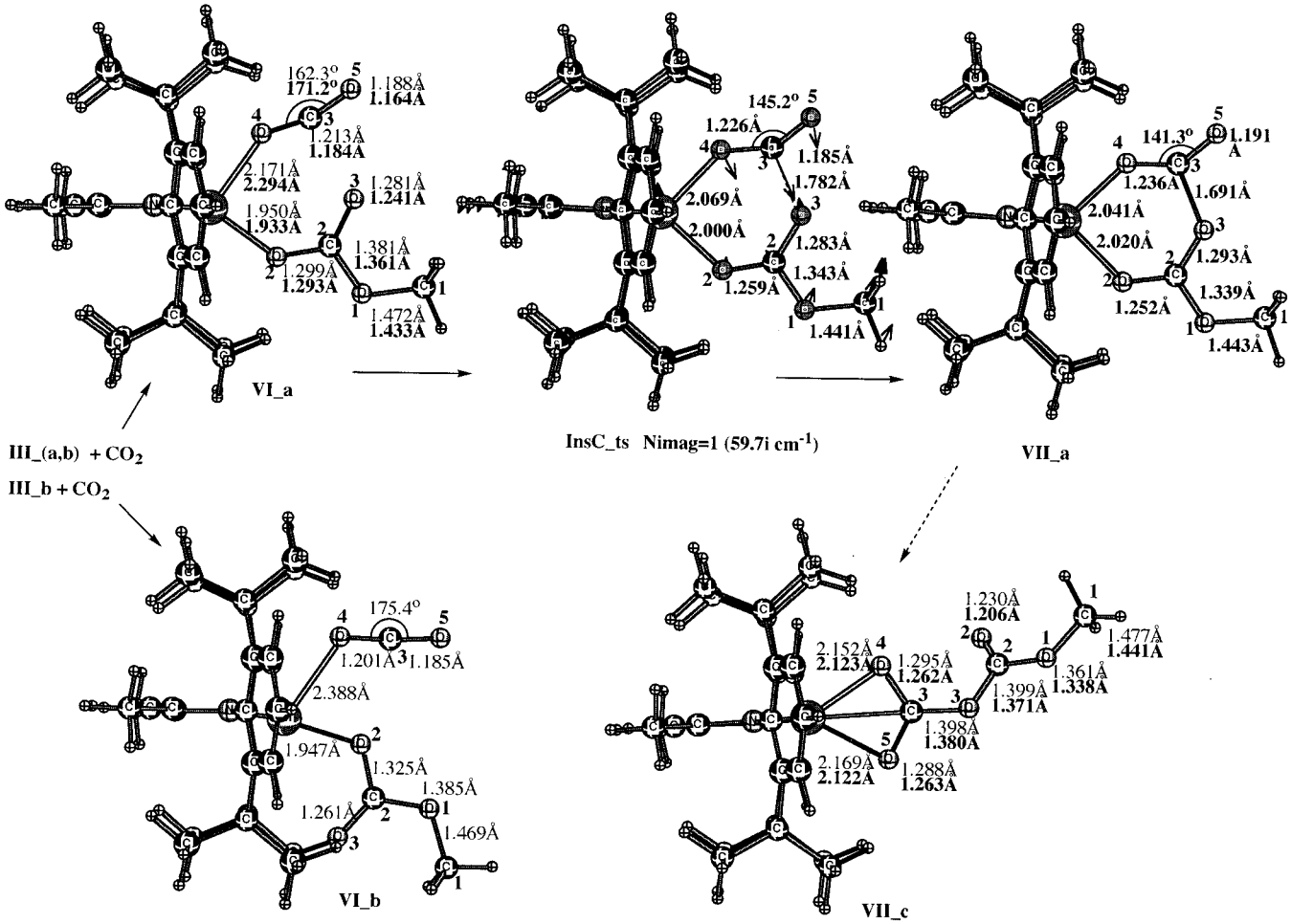

Figure 3. ONIOM(B3LYP:PM3) optimized structures of intermediates and TSs in insertion C of the CO_2/OC_2H_4 copolymerization catalyzed by (BDI)$ZnOCH_3$. Lightface numbers indicate bond lengths and bond angles using BS I and boldface numbers those using BS II.

Zn−OCO distance of 2.497 Å. This optimized structure has a distorted-tetrahedral four-coordinated Zn center, with the N−Zn−N chelate nearly perpendicular to the O−Zn−O plane. The OCO ligand, with end-on coordination to Zn through σ-donation, is still linear and cis to the methyl group. On comparison of the optimized structures of complexes **I** and **II** at the ONIOM(B3LYP/BS I:PM3) level of theory, the Zn−OCH_3 distance increases by 0.015 Å due to the increased number of ligands. The binding energy of CO_2 in complex **II** at the ONIOM(B3LYP/BS I:PM3) level is 1.7 kcal/mol, while no binding can be found at the ONIOM(B3LYP/BS II:PM3) level. The weak interaction between CO_2 and Zn indicates that CO_2 is not a good σ-donor.

For CO_2 insertion products, two equilibrium structures (the number of imaginary frequencies Nimag = 0) **III_a** and **III_b** were found. **III_a** appears first on the reaction pathway and then converts into **III_b** via the isomerization TS **III_iso_ts**. Structures **III_a** and **III_b** have tetrahedral Zn centers and chelating methyl carbonate ligands. In **III_a**, the Zn−O^2 σ-bond is formed at 1.991 Å. The Zn−O^1 bond is significantly weakened upon formation of the O^1−C^2 bond; the Zn−O^1 distance of 2.187 Å, which is 0.33 Å longer than that of complex **I**, indicates that the Zn−O^1 covalent σ-bond has been replaced by a σ-donative interaction between O^1 and Zn. The C^2−O^1CH_3 distance of 1.456 Å in **III_a** is slightly longer than a regular C−O single bond (i.e., 1.438 Å in **III_b**), due to the Zn···O^1 interaction. Because of the resonance effects between C−O^2 and C═O^3, the coordination-free carbonyl C═O^3 bond length of 1.212 Å is slightly longer than a regular C═O double bond (i.e., 1.209 Å in formic acid) and the C−O^2 distance of 1.285 Å is substantially shorter than a C−O single bond. With **III_a** as a starting point, the more stable complex **III_b** can be formed through the TS of isomerization, **III_iso_ts**. This TS is a 16e unsaturated species, with a coplanar tricoordinated structure, where the Zn···O^1 chelative interaction has been broken and the rotation of C═O^3 and C−O^1CH_3 around C−O^2 has taken place in preparation for a more intuitive and stronger bond between Zn and O^3. The frequency calculation of **III_iso_ts** gives one imaginary frequency of 61.8i cm^{-1}, and the corresponding normal mode clearly indicates the nature of the reaction coordinate, as indicated by arrows in Figure 1. In **III_b**, O^2 and O^3 serve as coordinated atoms in the chelating methyl carbonate ligand and the O^1CH_3 group becomes free from coordination. The C^2−O^1 bond of 1.342 Å is 0.11 Å shorter than that of **III_a** and also slightly shorter than a regular single-bond distance, due to resonance effects. In comparison with the structure of **III_a**, where the σ-bond of Zn−O^2 is 0.196 Å shorter than the chelative σ-donation bond of Zn−O^1, O^2 and O^3 in **III_b** are more evenly bound with Zn. The Zn−O^2 distance is nearly equal to the average of two Zn−O distances in **III_a**, while the Zn−O^3

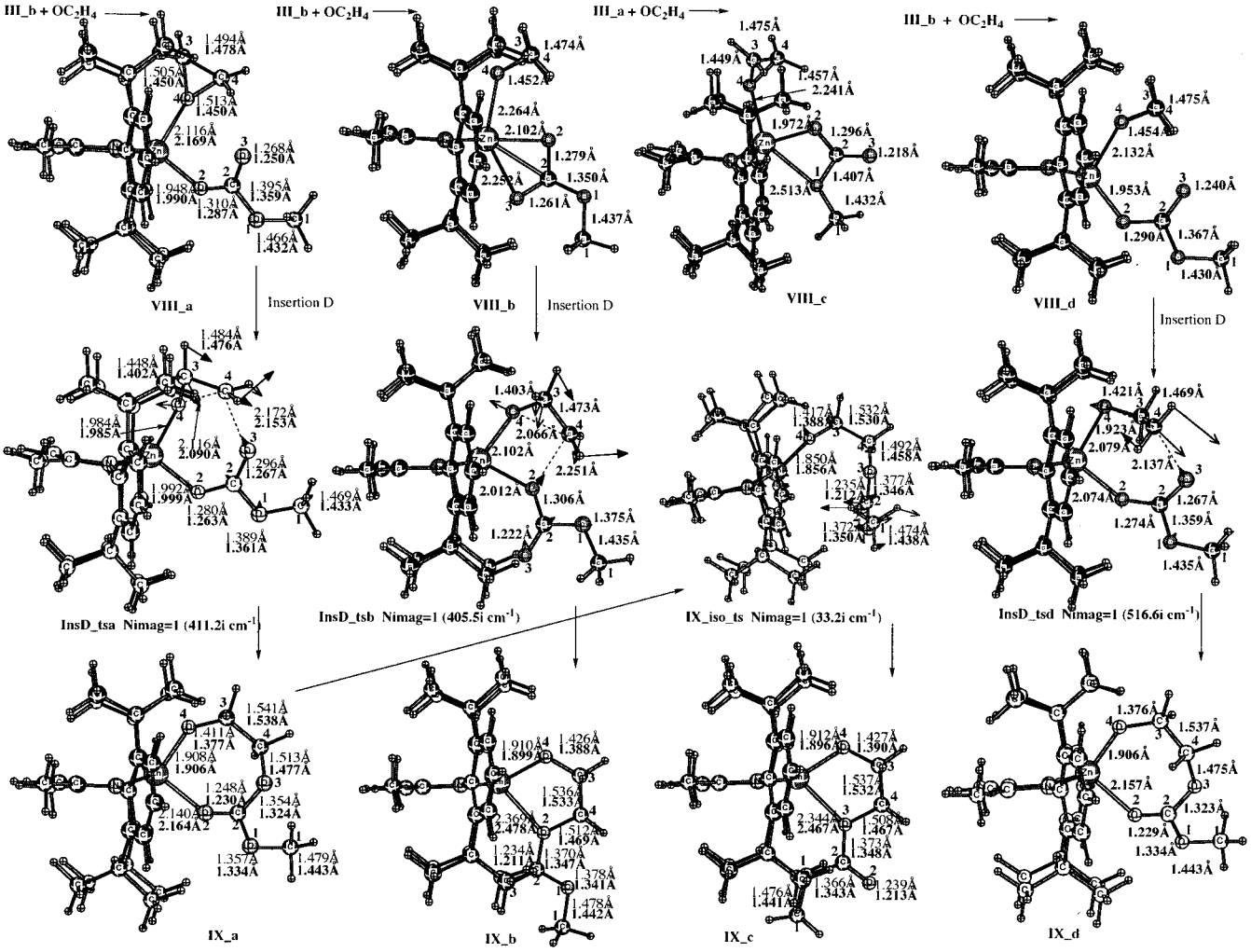

Figure 4. ONIOM(B3LYP:PM3) optimized structures of intermediates and TSs in insertion D of the CO_2/OC_2H_4 copolymerization catalyzed by (BDI)$ZnOCH_3$. Lightface numbers indicate bond lengths and bond angles using BS I and boldface numbers those using BS II.

distance is 0.03 Å longer than the $Zn-O^2$ distance because of the cis influence of the methyl group. The C^2-O^2 and C^2-O^3 bonds are also nearly equal to each other at 1.273 and 1.277 Å, respectively. The structure indicates a stronger resonance effect in $O^2-C^2-O^3$, which has stabilized complex **III_b** over **III_a** by 3.3 kcal/mol (see Table 2).

Although coordination of CO_2 to complex **I** is energetically unfavorable, insertion of CO_2 into the $Zn-OCH_3$ bond is found to be an exothermic process. As shown in Table 2, the ONIOM(B3LYP/BS II:PM3) energies without ZPE of **III_a** and **III_b**, relative to the reactants **I** + CO_2, are −18.8 and −22.1 kcal/mol, respectively. At 1 atm and 298.15 K, which is close to the experimental reaction temperature, the Gibbs free energy changes from **I** + CO_2 to the insertion products **III_a** and **III_b** are −5.8 and −11.0 kcal/mol, respectively, indicating that insertion of CO_2 is exothermic also in Gibbs free energy. The activation barrier and free energy at **III_iso_ts** for isomerization of the carbonate complex **III_a** to **III_b** are 9.3 and 8.4 kcal/mol, respectively, which reflect the energy requirements for breaking the $Zn-O^1CH_3$ bond.

We have also tried to locate the TS **InsA_ts** for CO_2 insertion into the Zn−methoxy bond. TS searches with BS I from several different initial structures, including a structure with a large OCO−Zn distance of 3.00 Å, have systematically converged to the CO_2 insertion product **III_a**. As mentioned above, optimizations of prereaction complex **II** using BS II also tend to converge to **III_a**; the energy smoothly goes down from **I** + CO_2 to the limit of **III_a** during the optimization. Geometrical changes during the optimization show that the approach of OCO to Zn occurs simultaneously with bending of the linear OCO and attack of O^1 in the methoxy ligand to C in OCO. Finally, in **III_a**, the O−C−O angle has become around 120° from the original 180°. The OCH_3 group has been pushed away but is still weakly bound together with Zn. Two new bonds, the $Zn-O^2$ σ-bond and the O^1-C^2 bond, are formed. We conclude that CO_2 insertion into the Zn−methoxy bond takes place without barrier with BS II and a negligibly small barrier with BS I.

B. Ethylene Oxide Insertion into the Zinc−Alkoxyl Bond. The coordination of ethylene oxide through σ-donation from the lone pair of OC_2H_4 to Zn of (BDI)$ZnOCH_3$ (**I**) forms either parallel complex **IV_a** or perpendicular complex **IV_b**. As shown in Figure 2, the optimized structures of both **IV_a** and **IV_b** have distorted-tetrahedral Zn centers with O−Zn−O angles close to 90°. The $Zn-O^1CH_3$ bonds are elongated from 1.852 Å in **I** to 1.896 and 1.899 Å in **IV_a** and **IV_b**,

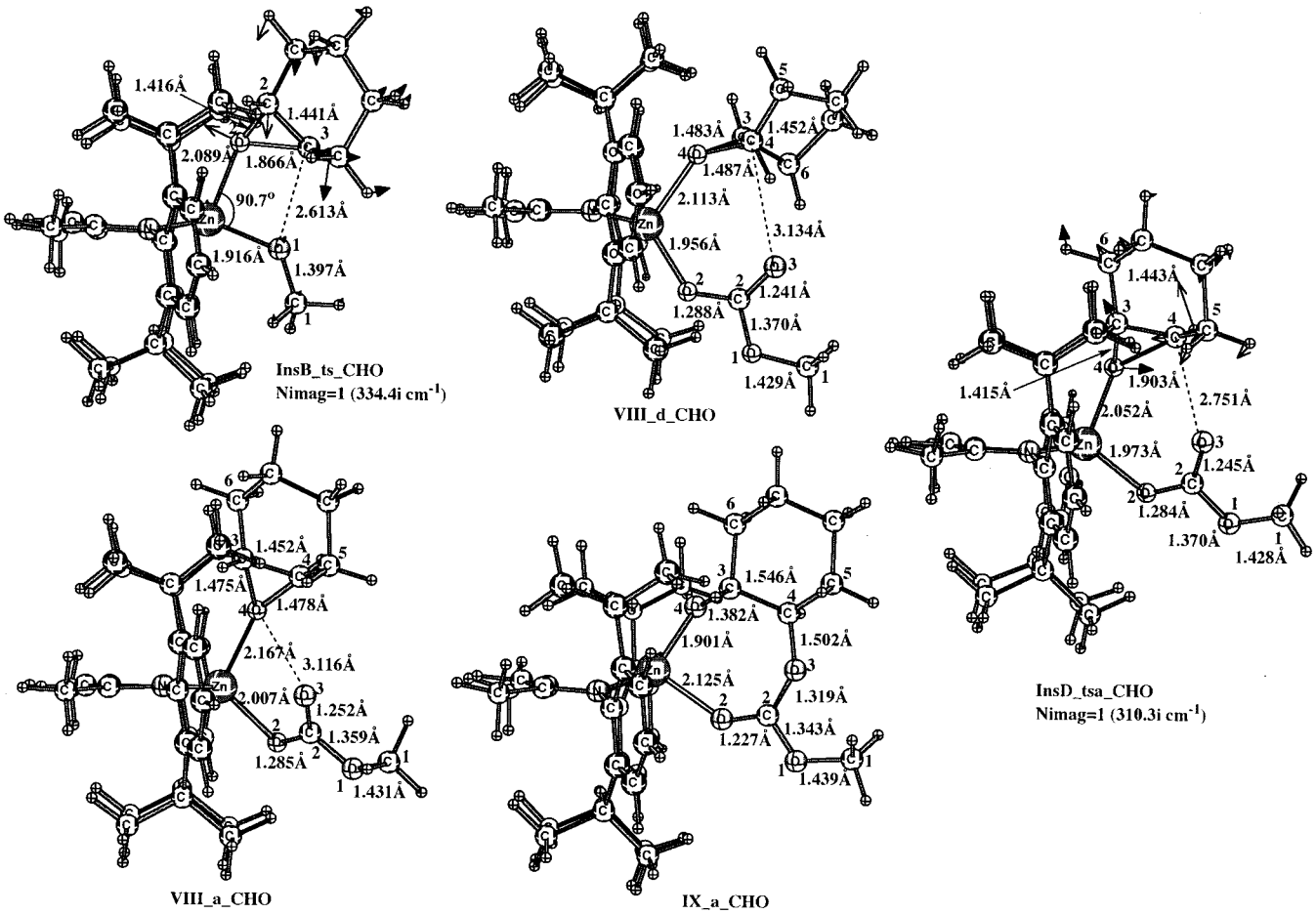

Figure 5. ONIOM(B3LYP/BS II:PM3) optimized structures of intermediates and TSs for reactions of cyclohexene oxide: **InsB_ts_CHO**, **VIII_(a,d)_CHO**, **IX_a_CHO**, and **InsD_tsa_CHO**.

respectively. It is clear from the $Zn-O^2C_2H_4$ distance of 2.201 Å in **IV_a** and 2.187 Å in **IV_b** that OC_2H_4 is more strongly bound to Zn perpendicularly than parallel. These geometrical parameters suggest that binding of OC_2H_4 with **I** is much stronger than that of CO_2. From **I** to **IV**, the methyl group has rotated from the N−Zn−N plane to the perpendicular O−Zn−O plane and is trans to the coordinated OC_2H_4 in both **IV_a** and **IV_b**. The C−O distances in OC_2H_4 have increased from 1.435 Å in a free molecule to 1.448−1.461 Å in **IV,** while the C^2-C^3 distance is nearly unchanged from free OC_2H_4. In the parallel complex **IV_a**, the C^3-O^2 bond closer to the OCH_3 group is 0.013 Å longer than the other C^2-O^2 bond. In perpendicular complex **IV_b**, the difference between the two C−O bonds is smaller. At the ONIOM(B3LYP/BS II:PM3) level of theory, the binding energy of OC_2H_4 to complex **I** is 12.7 kcal/mol for parallel complex **IV_a** and 15.5 kcal/mol for perpendicular complex **IV_b**. The ONIOM energy difference **IV_a** − **IV_b** of 2.8 kcal/mol mainly comes from the ΔE(high,model) contribution, i.e., the B3LYP energy difference of the small model system, which is 2.5 kcal/mol. The ΔE(PM3,model) and ΔE(PM3,real) of **IV_a** − **IV_b** are 1.2 and 1.5 kcal/mol, respectively, and they nearly cancel out. It is probable that the larger steric repulsion between the bulky substituents and ethylene oxide in **IV_a** than in **IV_b** affects the optimization so that a longer Zn−oxygen distance and weaker interaction are obtained. There should be a transition state connecting **IV_a** and **IV_b**. This TS would involve rotation of OC_2H_4 around its O^2-C^2 axis and have a low barrier; we did not determine its structure.

The coordination energies (12.7−15.5 kcal/mol) of OC_2H_4 to complex **I** are smaller than the Pd−olefin or Pd−carbon monoxide complexation energies (20−40 kcal/mol) studied previously,[7] presumably mainly because these is no π-back-donation in the $Zn-OC_2H_4$ interactions as in Pd−olefin or Pd−carbon monoxide interactions, although the metals involved are also different. By taking into account the contribution of entropy, the Gibbs free energies of **IV_a** and **IV_b** at 1 atm and 298.15 K, relative to **I** + OC_2H_4, are +2.6 and +0.3 kcal/mol, respectively. Thus. under the experimental reaction conditions (20−50 °C, 1 atm), the OC_2H_4 coordination complexes are not likely to exist as stable intermediates.

Figure 2 also shows the optimized structures of the TS for OC_2H_4 insertion into the Zn−methoxy bond, **InsB_ts**, and of the insertion product, complex **V**. The frequency calculation on **InsB_ts** gives one imaginary frequency of 441.1i cm^{-1}, which represents the reaction coordinate shown by arrows in the figure. Although the intrinsic reaction coordinate (IRC) has not been followed, its parallel epoxide structure and the reaction coordinate suggest that **InsB_ts** connects the parallel OC_2H_4 coordination complex **IV_a** and the insertion product **V**. In **InsB_ts**, the O^2-C^3 distance, 1.965 Å, has stretched more than 30% from the reactant **IV_a**, while the forming bond O^1-C^3 of 2.235 Å is still nearly 0.8 Å longer than that of the product **V**. The most important

Table 2. Total Energies and Free Energies (in au, in Italics) of Reference Compounds, Relative Energies Δ*E* (in kcal/mol). and Relative Free Energies Δ*G* (at 298.15 K, 1 atm, in kcal/mol) of Optimized Intermediates and TSs for the Reaction of CO_2 and C_2H_4O or $C_6H_{10}O$ (with _CHO Label after the Slant) at the ONIOM(B3LYP/BS II:PM3) Level, Relative to complex I + Appropriate Number of CO_2, C_2H_4O, or $C_6H_{10}O$

compd	*E* and Δ*E*	*G* and Δ*G*
CO_2	*−188.622 07*	*−188.631 09*
$C_2H_4O/C_6H_{10}O$	*−153.813 0/ −309.826 87*	*−153.779 82/ −309.704 97*
I	*−407.575 95 (−1 419.868 7)*[a]	*−406.969 753*
	0.0/0.0	0.0
III_a	−18.8	−5.8
III_iso_ts	−9.5	2.6
III_b	−22.1	−11.0
IV_a	−12.7	2.6
IV_b	−15.5	0.3
InsB_ts/InsB_ts_CHO	17.8/−0.8	30.9/12.8
V	−39.6	−22.6
VI_a	−18.6	3.7
InsC_ts	−16.9	5.1
VII_a	−17.0	4.6
VII_c	−10.2	12.4
VIII_a/VIII_a_CHO	−29.8 (−26.8[a])/−29.7	−2.7/−1.7
VIII_b	−30.1	−1.5
VIII_c	−30.0	−3.0
VIII_d/VIII_d_CHO	−30.9/−28.6	−2.5/−
InsD_tsa/InsD_tsa_CHO	9.7 (11.6)/−20.2	34.9/6.2
InsD_tsb	9.2	34.4
InsD_tsd	5.4	29.9
IX_a/IX_a_CHO	−35.1 (−36.5)/−65.0	−6.6/−37.8
IX_b	−31.1	−3.9
IX_c	−34.2	−6.2
IX_d	−34.7	−7.4
IX_iso_ts	−27.0	1.4

[a] Numbers in parentheses are single-point energies calculated at the standard B3LYP/BS II level at the ONIOM optimized geometries.

reaction coordinates at **InsB_ts** are breaking of the O^2-C^3 bond (ring opening) and forming of the $Zn-O^2$ σ-bond, which are followed by forming of the O^1-C^3 bond (nucleophilic addition) and breaking of the $Zn-O^1$ σ-bond. These results indicate that ring opening and nucleophilic addition are taking place asynchronously, with the latter following the former. **InsB_ts** is a TS that retains the C^3 stereochemistry; the breaking O^2-C^3 and forming O^1-C^3 bonds are on the same side of the C^2-C^3 bond.

The insertion product, **V**, has also a tetrahedral Zn center and a chelating alkoxyl ligand. The $Zn-O^2$ σ-bond is formed at 1.910 Å, and the $Zn-O^1$ σ-bond of 1.85−1.90 Å in complex **I**, **IV_a**, or **IV_b** has been replaced by the chelative interaction between O^1 and Zn at 2.237 Å. $Zn-O^2$ can be considered as a covalent bond, while the $Zn-O^1$ interaction mainly comes from the σ-donation from the lone pair of O to the vacant orbital of Zn. Due to the interaction between O^1 and Zn, the O^1-C^3 and O^1-C^1 bonds, especially the first one, are weakened. The O^1-C^3 and O^1-C^1 bonds are 1.446 and 1.423 Å, which are both slightly longer than a regular C−O bond distance such as $O^2-C^2 = 1.391$ Å. The $O^2-C^2-C^3-O^1$ dihedral angle is about 50°, which indicates the gauche conformation of C^2-O^2 and C^3-O^1 bonds.

The barrier at **InsB_ts**, measured from the complex **IV_a**, is 30.5 kcal/mol in potential energy or 28.3 kcal/mol in Gibbs free energy at 1 atm and 298.15 K, respectively. Since **IV** is not stable in free energy, the activation free energy should be measured from the stable starting complex, **I**; the activation free energy from **I** to **InsB_ts** is 30.9 kcal/mol. The energy of the product, relative to **I** + OC_2H_4, is −39.6 kcal/mol in potential energy or −22.6 kcal/mol in free energy. Although the reaction is highly exothermic, there is a high barrier between the prereaction complex and the insertion product. The high barrier is caused by the very asynchronous nature of the transition state **InsB_ts**. The O^2-C^3 bond in ethylene oxide has already been broken, but the nucleophilic attack to form the O^1-C^3 bond between the methoxy oxygen and ethylene oxide carbon has not yet taken place. Obviously, doing these two at the same time is energetically unfavorable, presumably due to the overcrowding in the reaction region.

In a brief summary of insertions A and B, from the free energy point of view, the coordination complex of neither CO_2 nor OC_2H_4 is a thermodynamically stable intermediate. This is probably due to lack of π-back-donation between either CO_2 or OC_2H_4 with Zn. However, both insertion reactions are exothermic, and OC_2H_4 insertion is over 10 kcal/mol more exothermic than CO_2 insertion. Despite the thermodynamic preference for the OC_2H_4 insertion reaction, the kinetic preference strongly favors the barrierless insertion of CO_2 over the insertion of OC_2H_4, which requires an activation free energy of around 30 kcal/mol.

C. CO_2 Insertion into the Zinc−Carbonate Bond. For CO_2 coordination to the Zn carbonate complex **III_a** or **III_b**, the two coordination complexes **VI_a** and **VI_b**, as shown in Figure 3, are found. **VI_b** is found at the ONIOM(B3LYP/BS I:PM3) level of theory; however, optimization of this complex with BS II results in the dissociation of CO_2. The structures of both BS I complexes appear to have tetrahedral Zn centers; the coordination of CO_2 to Zn is accompanied by breaking of one relatively weaker Zn−O interaction, i.e., $Zn-O^1$ in **III_a** or $Zn-O^3$ in **III_b**. As shown in the drawings of **III_a** and **III_b** in Figure 1, the front-side or back-side attack in these structures is defined as CO_2 approaching Zn from the weaker $Zn-O^{1\text{ or }3}$ bond side or the stronger $Zn-O^2$ bond side, respectively. Therefore, complexes **VI_a** and **VI_b** in Figure 3 are the result of the front-side and back-side coordination of CO_2 to **III_b** accompanied by the breaking of the $Zn-O^3$ interaction, respectively. We have also tried to locate the anticipated coordination complex from the back-side attack of CO_2 at **III_a**. The structure of this complex should be similar to that of **VI_b** but with the $-C^2-O^1CH_3$ group cis and the $-C^2-O^3$ group trans to the Zn center as they are in complex **III_a**. However, geometry optimization from such an initial structure converges to **VI_a**, where the inversion of the $Zn-O^2-C^2$ bond takes place due to repulsion between the bulky substituents and the methoxy group. Thus, we could link **VI_a** to either **III_a** or **III_b**. The front-side attack of CO_2 at **III_a** is not considered for two reasons: (1) the coordination of CO_2 to Zn is sterically impeded by the methoxy group and (2) the resulting complex, which

has $C^2-O^1CH_3$ instead of $C^2=O^3$ cis to the coordinated CO_2, is not appropriate for insertion of CO_2.

In **VI_a**, the newly formed $Zn-O^4CO$ bond of 2.294 Å is 0.11 or 0.18 Å longer than the $Zn-O^1(Me)CO_2$ or $Zn-O^3C(O)OMe$ distance in **III_a** or **III_b**, respectively. On the other hand, the $Zn-O^2$ distance in **VI_a** is 0.06 or 0.15 Å shorter than the $Zn-O^2$ distance in **III_a** or **III_b**, respectively. The weakening of one Zn−O bond causes strengthening of the other Zn−O bond. The O−C−O angle bends from 180.0 to 171.2° in **VI_a**. The O^4-C^3 bond has elongated while the O^5-C^3 bond has shortened by 0.01 Å from the O−C distance in free CO_2. Due to the breaking of the $Zn-O^1$ (or $Zn-O^3$) interaction and strengthening of the $Zn-O^2$ bond on going from **III_a** (or **III_b**) to **VI_a**, the O^2-C^2, C^2-O^3, and C^2-O^1 distances also undergo changes (shown in Figures 1 and 3). The overall structural feature of **VI_b** is similar to that of **VI_a**. Since **VI_b** has not been found as a stable complex at the ONIOM(B3LYP/BS II:PM3) level of theory, we will not discuss its structure in detail.

The potential energy of complex **VI_a** is 0.2 and 3.5 kcal/mol higher than **III_a** + CO_2 and **III_b** + CO_2, respectively. This negative coordination energy of the second CO_2 suggests that there is a transition state connecting **III_a** or **III_b** to **VI_a**. The increase in energy upon coordination is due to the breaking of a Zn−O bond during coordination of CO_2 to **III_a** or **III_b**. Considering that this process does not involve major bond reorganization, the barrier is expected to be small and we did not try to locate it. The Gibbs free energy of **VI_a** is 3.7 kcal/mol relative to **I** + $2CO_2$, i.e., 9.5 and 14.7 kcal/mol higher than **III_a** + CO_2 and **III_b** + CO_2, respectively; these CO_2 complexes are not thermodynamically stable intermediates.

From complex **VI_a**, the insertion of CO_2 can proceed via TS **InsC_ts**, leading to the chelating insertion product **VII_a**. **InsC_ts** has one imaginary frequency of 59.7i cm^{-1}, and the corresponding normal mode shown in Figure 3 indicates bond formation between C^3 and O^3. The insertion of carbon dioxide ($O^3=C^3=O^4$) into Zn-carbonate bond occurs with the canonical structure change

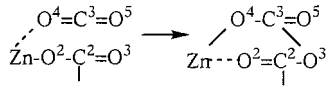

The $Zn-O^2$ σ bond, $C^2=O^3$ π bond, and $C^3=O^4$ π bond in **IV_a** are replaced by a $Zn-O^4$ σ bond, C^3-O^3 σ bond, and $C^2=O^2$ π bond in **VII_a**, and the Zn- - -O^4 donative bond by the $Zn-O^2$ donative bond. The geometrical parameters, including the $O^4-C^3-O^5$ angle of 145.2° and the C^3-O^3 distance of 1.782 Å, which are only 4° and 0.09 Å larger than that in the product **VII_a**, suggest that **InsC_ts** is rather a late TS. In **VII_a** the newly formed C^3-O^3 bond is weak, with a long bond distance of 1.691 Å.

The activation potential energy and free energy at **InsC_ts** are 1.9 and 10.9 kcal/mol measured from the starting stable intermediate **III_a**. The reverse barrier for dissociation of CO_2 from the product **VII_a** is 0.1 or 0.5 kcal/mol in free energy. The insertion product, **VII_a**, lies 1.8 kcal/mol in potential energy and 10.4 kcal/mol in free energy above the starting complex **III_a**. Thus, under the experimental conditions, the free energy indicates that this reaction is reversible and should reach equilibrium easily with the intermediate **III_a** + CO_2 to be much more favored over the insertion product **VII_a**.

Starting from the backside coordination complex **VI_b**, direct insertion of CO_2 into the $Zn-O^2$ bond through formation of the C^3-O^2 bond would lead to complex **VII_b**, which, as suggested in Scheme 1, is expected to have $\alpha-\gamma$ chelative interaction between the bicarbonate ligand and Zn. However, geometry optimization from such an initial structure converges back to **VI_b** at the ONIOM(B3LYP/BS I:PM3) level and converges all the way back to **III_b** at the ONIOM(B3LYP/BS II:PM3) level. These facts indicate that direct insertion of CO_2 into the Zn−O bond does not take place.

The optimized structure of another type of Zn−bicarbonate complex, **VII_c**, which can be obtained from isomerization of **VII_a**, is also shown in Figure 3. In **VII_c**, the carbonate group acts as a chelating ligand, which provides α- and γ-oxygen to the tetrahedral Zn center. The structure is basically analogous to the structure of **III_b**, another chelating carbonate complex; the $Zn-O^4$ and O^4-C^3 distances are nearly equal to the $Zn-O^5$ and O^5-C^3 distances, respectively. Unlike **III_b**, where the methyl group is found to be coplanar with $O^1C^2O^3$, **VII_c** has a $O^4-C^3-O^3-C^2$ dihedral angle of −32.9°, presumably due to the electrostatic repulsion between two carbonyl groups. As a consequence of the nonplanar structure, the delocalization of π electrons among C−O bonds is reduced. In **VII_c**, the O^4-C^3 and O^5-C^3 distances are 0.01 Å shorter than the $O^{2\text{ or }3}-C^2$ distances in **III_b**, and the C^3-O^3 distance is 0.04 Å longer than the C^2-O^1 distance in **III_b**. The $Zn-O^{4,5}$ interactions are therefore weakened due to strengthening of the $O^{4,5}-C^3$ bonds. The π-bond in $O^3C^2=O^2(OCH_3)$ group of **VII_c** is also more localized than that of **VII_a**, with a C^2-O^2 bond of 1.206 Å, which is ∼0.05 Å shorter than C^2-O^2 of **VII_a**. Complex **VII_c** lies 12.4 kcal/mol higher than the reference, **I** + $2CO_2$, on the overall free energy surfaces. **VII_c** is 7.8 kcal/mol higher in free energy than **VII_a**, due to the decreased resonance effect in **VII_c**. We did not look for the TS connecting **VII_a** and **VII_c**.

As a brief conclusion for insertion C, both coordination complexes and insertion products are energetically less stable than the reactants, **III_(a,b)** + CO_2, in either potential energy or free energy. With the absence of a stable CO_2 coordination intermediate, the CO_2 insertion process from the intermediate **III_a** to product **VII_a** requires an activation free energy of 10.9 kcal/mol and is endothermic by 10.4 kcal/mol. The reverse barrier for dissociation of CO_2 from the insertion product **VII_a** is only 0.5 kcal/mol, and therefore an easy equilibrium is expected with the noninserted reactant **III_a** strongly favored over the insertion product.

D. Ethylene Oxide Insertion into the Zinc−Carbonate Bond. Starting from the Zn−carbonate complexes **III_(a,b)**, the coordination of OC_2H_4 from either the front side or the back side results in various conformations of parallel or perpendicular coordination complexes. We have obtained four coordination complexes and found that the difference in complexation energy between front-side and back-side coordination or between parallel and perpendicular coordination is

within 1−2 kcal/mol. Although we have not attempted to exhaust all possible conformations, our results should be quite reliable. The optimized structures of the coordination complexes **VIII_(a,b,c,d)** at the ONIOM-(B3LYP/BS II:PM3) level are shown in Figure 4. **VIII_a** and **VIII_d** are parallel and perpendicular complexes, respectively, resulting from the front-side coordination of OC_2H_4 to **III_b** accompanied by breaking of the $Zn-O^3$ bond. The front-side coordination of OC_2H_4 to **III_a** is again not considered for the same reasons discussed above for the CO_2 coordination. The back-side coordination of OC_2H_4 to **III_b** accompanied by breaking of the $Zn-O^3$ bond also results in both parallel and perpendicular complexes. However, only perpendicular complex **VIII_b** is found at the ONIOM(B3LYP/BS II:PM3) level of theory. Similarly, only parallel coordination complex **VIII_c** from the back-side attack of OC_2H_4 to **III_a** is found.

The optimized structures of **VIII_a** and **VIII_d** have tetrahedral Zn centers. Similar to CO_2 coordination, coordination of OC_2H_4 results in breaking of the $Zn-O^3$ interaction in **III_b**. When **VIII_a** and **VIII_d** are compared, the perpendicular complex **VIII_d** is again more stable than the parallel complex with a $Zn-O^4$ bond length of 2.132 Å, which is 0.037 Å shorter than that of **VIII_a**. The situation is similar to the case of the parallel and perpendicular coordination complexes **IV_a** and **IV_b**. However, the difference in binding energy, 1.1 kcal/mol, is 1.7 kcal/mol smaller than the 2.8 kcal/mol difference of **IV_a** − **IV_b**. The perpendicular coordination results in the nearly coplanar structure of $O^2-C^2=O^3$ with $Zn-O^4$ at a dihedral angle of −2°. In the parallel coordination complex, the corresponding $C^2-O^2-Zn-O^4$ dihedral angle is 67°. Due to the repulsion between the OC_2H_4 group with the coplanar $C^2=O^3$, the O^4-Zn-O^2 and $Zn-O^2-C^2$ angles in **VIII_d** are 7 and 13° larger than those in **VIII_a**, respectively.

The optimized structures **VIII_b** and **VIII_c** have five-coordinate Zn centers. The coordination of OC_2H_4 to **III_(a,b)** does not result in complete breaking but significant weakening of the $Zn-O^{1\text{ or }3}$ bond. Structures of **VIII_b** and **VIII_c** are similar to those of **VIII_a** and **VIII_d**, and will not be discussed in detail.

The energies of **VIII_a**, **VIII_b**, and **VIII_d**, relative to **III_b** + OC_2H_4, are −7.7, −8.0 and −8.8 kcal/mol, respectively. The energy of **VIII_c**, relative to **III_a** + OC_2H_4, is −11.2 kcal/mol. The coordination energies are about 2−8 kcal/mol smaller than those of complex **I**, 12.7−15.5 kcal/mol. The difference comes from the fact that the coordination of OC_2H_4 to complex **III_(a,b)** requires additional energy to break the chelative $Zn-O^{1,3}$ interaction. The free energies of **VIII_a**, **VIII_b**, and **VIII_d**, relative to **III_b** + OC_2H_4, are 8.3, 9.5, and 8.5 kcal/mol, respectively, and the coordination of OC_2H_4 to complex **III_(a** or **b)** is an endothermic process. The free energy of **VIII_c** also lies above that of **III_a** + OC_2H_4 by 2.8 kcal/mol. These complexes are therefore not stable intermediates.

In front-side coordination complex **VIII_a** or **VIII_d**, the carbonyl group $C^2=O^3$ is cis to the coordinated OC_2H_4. The ring opening of the ethylene oxide followed by the nucleophilic addition of O^3 to C^4 leads to a seven-membered chelating ring product, **IX_a** or **IX_d**, respectively. In the insertion products, the $-O^4-C^3-C^4-O^3-C^2=O^2$ chain is a chelating ligand in which O4 forms a covalent bond with Zn and O^2 donates σ-electrons to the Zn center. The TSs, **InsD_tsa** and **InsD_tsd**, which are retention and inversion TSs, respectively, for the ring-opening and nucleophilic addition of ethylene oxide, are found to link **VIII_a** with **IX_a** and **VIII_d** with **IX_d**, respectively. For the ring-opening and nucleophilic addition, there are two groups of reaction coordinates: (1) breaking of the O^4-C^4 bond and forming of the $Zn-O^4$ σ-bond and (2) forming of the C^4-O^3 bond, moving of the π-bond from $C^2=O^3$ to C^2-O^2 and breaking of the $Zn-O^2$ σ-bond. In the retention TS **InsD_tsa**, the breaking bond O^4-C^4 is elongated by 0.64 Å from 1.450 Å of the reactant **VIII_a** and the $Zn-O^4$ σ-bond is starting to be formed with a bond length of 1.985 Å, which is 0.184 Å shorter than that of **VIII_a** and 0.079 Å longer than that of **IX_a**. Therefore, **InsD_tsa** is rather late in the ring-opening process. On the other hand, the inversion TS **InsD_tsa** is at the early stage of the nucleophilic addition process. The forming bond C^4-O^3 in **InsD_tsa** is still 0.68 Å longer than in the insertion product **IX_a**. Also in **InsD_tsa**, the $C^2=O^3$ bond is 0.017 Å longer and 0.057 Å shorter, the C^2-O^2 bond is 0.024 Å shorter and 0.033 Å longer, and the $Zn-O^2$ bond is 0.009 Å longer and 0.165 Å shorter than that of the reactant **VIII_a** and the product **IX_a**, respectively. For **InsD_tsd**, the breaking O^4-C^4 bond of 1.923 Å, which is 0.47 Å longer than that of the reactant **VIII_d**, suggests that the ring-opening process is also in its late stage but earlier than that in **InsD_tsa**. The changes in the bond distances of the C^4-O^3, O^3-C^2, and C^2-O^2 bonds are similar to those in **InsD_tsa**. However, the status of formation of the $Zn-O^4$ σ-bond and breaking of the $Zn-O^2$ σ-bond are different from **InsD_tsa**. In **InsD_tsd**, the $Zn-O^4$ and $Zn-O^2$ bonds are closer to the reactant and the product, respectively, which is in contrast with that of **InsD_tsa**.

In the back-side perpendicular coordination complex **VIII_b**, the carbonyl group $C^2=O^3$ is trans to the coordinated ethylene oxide. Thus, the ring opening of ethylene oxide is followed by the nucleophilic addition of O^2 to C^4 and leads to a five-membered-ring chelative complex, **IX_b**. Starting from **VIII_b**, the ring opening and the nucleophilic addition can only proceed through retention stereochemistry, since O^2 is bound to the Zn center on the same side of theC^3-C^4 bond with O^4. The optimized structure of the TS, **InsD_tsb**, is also shown in Figure 4. As can be seen from the geometries of both the TS and the coordination complex, **InsD_tsb** is more likely to connect a parallel coordination complex and the product. However, on the basis of previous discussions, we did not locate the parallel complex, as it presumably has a structure and coordination energy similar to those of the perpendicular complex **VIII_b**. Therefore, we connect the perpendicular complex **VIII_b** with **InsD_tsb**. In **InsD_tsb**, the ring opening of ethylene oxide is again in its late stage, with the breaking O^4-C^4 bond being 0.61 Å longer than that of the reactant **VIII_b**. The forming bond C^4-O^2 is 0.78 Å longer than that of the product **IX_b**.

Frequency calculations have been performed on the three TSs. The imaginary modes of 411.2i, 405.5i, and

516.6i cm^{-1}, representing the reaction coordinates in **InsD_tsa**, **InsD_tsb**, and **InsD_tsd**, respectively, are shown in Figure 4. The activation barriers at **InsD_tsa**, **InsD_tsb**, and **InsD_tsd**, measured from **VIII_a**, **VIII_b**, and **VIII_d**, are 39.5, 39.3, and 36.3 kcal/mol in potential energy. Since **VIII**'s are not stable intermediates in free energy, the activation free energy should be measured from the stable intermediate **III_a** or **III_b**. The activation free energy for various TSs **InsD_ts(a,b,d)** from **III_a** or **III_b** is in the range of 35−45 kcal/mol, indicating that this insertion reaction cannot take place at room temperature.

Very similar features on both structures and energetics are found among the three TSs for insertion D and the TS for insertion B. The ring opening, which requires a rather high activation energy, is considered as the rate-limiting step. The nucleophilic attack from either the O atom in Zn−O or the O^3 atom in $Zn-O^2-C^2=O^3$ to C^4 takes place quite easily after the ring has opened. Since the barrier comes mainly from the breaking of the O^4-C^4 bond, the mode of the nucleophilic attack, either inversion or retention or either O^2 or O^3 attack, has only a small influence on the activation barrier. Therefore, we did not attempt to locate any TS of insertion D from coordination complex **VIII_c**.

Both insertion products **IX_a** and **IX_d** have seven-membered-ring chelating structures. The bond lengths and bond angles are very similar in the two ring structures. They are enantiomers with small differences in torsional angles. The torsional angles going around the ring $C^2-O^2-Zn-O^4-C^3-C^4-O^3-C^2-O^2-Zn$ are 45.1, −26.7, 50.8, −87.2, 79.9, −8.6, and −51.4° for **IX_a** and 25.7, 2.6, 25.8, −83.6, 81.9, −6.5, and −45.3° for the enantiomer of **IX_d**. The methoxy group is coplanar with the $O^2C^2O^3$ plane in both **IX_a** and **IX_d**, residing trans to the O^4-Zn-O^2 plane. The major structural differences between **IX_a** and **IX_d** are in the dihedral angle around the O^2-Zn, $Zn-O^4$, and O^4-C^3 bonds in the vicinity of the Zn atom. Some dihedral angles of 90° or so suggest a substantial torsional strain in the seven-membered ring. **IX_a** and **IX_d** are very close to each other in relative stability (within 1 kcal/mol). Insertion D either from **VIII_a** to **IX_a** or from **VIII_d** to **IX_d** is an exothermic process in free energy by 4−5 kcal/mol.

In the structure of five-membered-ring insertion product **IX_b** or its five-membered-ring isomer **IX_c**, the $-O^4-CH_2-CH_2-O^2$ group serves as a 1,4-chelating ligand. The $O^2-C^4-C^3-O^4$ dihedral angle of −53.9° indicates a gauche structure. The interaction between Zn and O^2 is weaker than the chelating interaction found in complex **V**, judging from the $Zn-O^2$ bond distances of 2.47−2.48 Å in **IX_b** or **IX_c** and 2.24 Å in **V**. The difference probably comes from the larger steric repulsion between the carbonate group in **IX_b** or **IX_c** with the bulky substituents on the diimine ligand. The weaker chelating interaction decreases the stability of complex **IX_b** or **IX_c**. Thus, the reaction **IV** → **V** is more than 25.0 kcal/mol more exothermic than the reaction **VIII_b** → **IX_b**. Complex **IX_b** lies 3.1 kcal/mol higher in energy than complex **IX_c**. **IX_c** has a stability similar to that of the seven-membered-ring insertion products **IX_a** and **IX_d**, with a relative energy of −34.2 kcal/mol (with respect to **I** + CO_2 + OC_2H_4).

Table 3. Calculated Reaction Energies and Experimental Enthalpies (in kcal/mol) for the Nucleophilic Addition of H_2O to Ethylene Oxide and Cyclohexene Oxide

	ΔE			
reacn	B3LYP/BS II[a]	MP2/BS II[b]	G2MS[c]	ΔH(exptl)[d]
$C_2H_4O + H_2O \rightarrow C_2H_6O_2$	−29.3 (−24.8)	−27.1	−21.8	−22.3, −23.9
$C_6H_{10}O + H_2O \rightarrow C_6H_{12}O_2$	−67.2 (−62.8)	−67.6	−62.5	

[a] The numbers in parentheses include ZPE corrections. [b] Single-point calculations at the B3LYP/BS II optimized geometries. [c] Single-point calculations at the B3LYP/6-31G(d) optimized geometries, including the B3LYP/6-31G(d) ZPE corrections. [d] Derived from experimental $\Delta H_f°$ from the NIST Chemistry WebBook: http://webbook.nist.gov.

The isomerization TS, **IX_iso_ts**, connecting the seven-membered-ring complex **IX_a** and the five-membered-ring complex **IX_c** is shown in Figure 4. In the structure of **IX_iso_ts**, the Zn center is tricoordinated coplanar, the chelative interaction of $Zn-O^2$ presented in **IX_a** is completely broken, and the carbonate group has rotated and moved away from Zn in order to facilitate the interaction between O^3 and Zn. The $Zn-O^4$ bond of 1.856 Å has shortened 0.05 Å from the reactant due to the decreased number of ligands. Frequency calculations give a unique imaginary mode of 33.2i cm^{-1}. The activation barrier at **IX_iso_ts**, measured from **IX_a**, is 8.1 kcal/mol.

E. Cyclohexene Oxide Insertion to the Zinc−Alkoxyl and Zinc−Carbonate Bonds. As discussed above, insertion B and insertion D for ethylene oxide require high activation energies and cannot take place at room temperature. These theoretical results are not consistent with the experimental observation that copolymerization of CO_2 and cyclohexene oxide takes place rather easily. Thus, we have to examine the reliability of using C_2H_4O as a model for $C_6H_{10}O$. Interestingly, experiments show that ethylene oxide does not undergo copolymerization with CO_2, which is consistent with our results for ethylene oxide.

To obtain information about the difference in the energetics between C_2H_4O and $C_6H_{10}O$, the reaction energies of the nucleophilic addition of H_2O to C_2H_4O and $C_6H_{10}O$ without catalyst were calculated at B3LYP/BS II, MP2/BS II, and G2MS levels of theory, as shown in Table 3. The experimental enthalpy is not available for the second reaction. Comparing the calculated energies for the first reaction with the experimental enthalpy (in the range −22.3 to −23.9 kcal/mol), one can see that G2MS yields the best result. Since our calculated ΔE(G2MS) for the first reaction deviates only 1−2 kcal/mol from the experimental enthalpy, we presume that our calculated energy of −62.5 kcal/mol at the G2MS level for the second reaction should be a very good estimate of the experimental enthalpy. Our results show that the ring-opening nucleophilic reaction of H_2O to cyclohexene oxide is thermodynamically as much as 40.7 kcal/mol more favorable than that to ethylene oxide. The other methods give very similar energy differences, 37.9 kcal/mol at B3LYP/BS II and 40.5 kcal/mol at MP2/BS II, both with the B3LYP/BS II ZPE correction. This suggests that the B3LYP/BS II method used in the present paper as the high level for the calculations with

the catalyst is giving reasonable energetics for the ring opening of the two epoxides. The difference most likely comes from the release of the six-membered-ring strain of cyclohexene oxide. The molecular structure of the product, 1,2-cyclohexanediol, has a perfect chair structure; therefore, no ring strain is present. However, in the structure of cyclohexene oxide itself, the perfect chair structure of the six-membered ring is distorted strongly, due to the three-membered epoxide ring. Thus, in addition to the three-membered-ring strain in structures of both ethylene oxide and cyclohexene oxide, there is also torsion and angle strain that is only present in the six-membered-ring structure of cyclohexene oxide. The release of the additional strain in cyclohexene oxide makes the nucleophilic addition of H_2O thermodynamically far more favorable than that to ethylene oxide. Hence, we also expect a lower activation energy and an earlier TS for the ring opening of cyclohexene oxide as compared to that of ethylene oxide.

In light of the above significant difference between the two model nucleophilic addition reactions, it is necessary to model the experimental Zn(II)-catalyzed CO_2 and epoxide copolymerization reaction with actual cyclohexene oxide as monomer. Unfortunately, reoptimizations at the ONIOM(B3LYP/BS II:PM3) level of all coordination complexes, TSs, and insertion products of insertion B and insertion D are not practical. Since various isomers of intermediates have been found above to have similar structures and energies, we recognize that we need to reoptimize only one cyclohexene oxide coordination complex, **VIII_CHO**, two TSs, **InsB_ts_CHO** and **InsD_ts_CHO**, and one insertion product, **IX_a_CHO**.

The optimized structures of the two insertion D coordination complexes, **VIII_a_CHO** and **VIII_d_CHO**, are shown in Figure 5. Complexes **VIII_a_CHO** and **VIII_d_CHO** are formed by parallel and perpendicular front-side coordination of $C_6H_{10}O$ to **III_b**. The structures of **VIII_a_CHO** and **VIII_d_CHO** resemble the optimized structures of C_2H_4O coordination complexes **VIII_a** and **VIII_d**, respectively. The $Zn-O^4$ distances are 2.167 Å in **VIII_a_CHO** vs 2.169 Å in **VIII_a** and 2.113 Å in **VIII_d_CHO** vs 2.132 Å in **VIII_d**. The O^4-C^3 and O^4-C^4 distances of coordination complexes **VIII_(a,d)_CHO** are also elongated by 0.02−0.03 Å from that of free $C_6H_{10}O$ due to the σ-donation from the O^4 lone pair to Zn. As was found in the coordination of C_2H_4O, the C^3-C^4 distances in the coordinated complexes and in free $C_6H_{10}O$ are almost the same. There is also no significant change of structural features of the six-membered ring before and after coordination. Obviously, the coordination of epoxide to Zn(II) forms weak complexes only through the σ-donation from the lone pair of the epoxide oxygen to Zn. The coordination energy of $C_6H_{10}O$ is similar to that of C_2H_4O. The energies of **VIII_a_CHO** and **VIII_d_CHO** lie −29.7 and −28.6 kcal/mol below the reference, **I** + CO_2 + epoxide, respectively, as compared with −29.8 and −30.9 kcal/mol of the C_2H_4O coordination complexes. Therefore, we should be able to predict also structures and complexation energies for other types of coordination complexes, such as complex **IV_CHO** formed by coordination of $C_6H_{10}O$ to complex **I**. We can conclude that the use of C_2H_4O instead of $C_6H_{10}O$ for coordination complexes gives quite reliable results on both structures and energetics.

IX_a_CHO is a seven-membered-ring product of insertion D of $C_6H_{10}O$. The structures of **IX_a** and **IX_a_CHO** are rather similar. The differences between their corresponding bond distances range from 0.005 to 0.04 Å. The six-membered ring in **IX_a_CHO** has a chair conformation with two C−O bonds at two equatorial positions. The dihedral angle $O^4-C^3-C^4-O^3$ of −75.4° is 15° larger in magnitude than the normal dihedral angle in a chair structure but is 12° smaller in magnitude than that of **IX_a**, a compromise between the strain of the six-membered cyclohexane ring and that of the seven-membered chelating ring. The dihedral angle of $C^5-C^4-C^3-C^6$ in the six-membered ring, 48.5°, is ∼12° smaller than the normal dihedral angle in a chair structure, another evidence of compromise. The energy of **IX_a_CHO** lies 65.0 and 35.3 kcal/mol below the references **I** + CO_2 + $C_6H_{10}O$ and **VIII_a_CHO**, respectively. When the entropy contribution is counted in, the free energy change at 298.15 K and 1 atm from **VIII_a_CHO** to **IX_a_CHO** is −36.1 kcal/mol. Therefore, insertion D of $C_6H_{10}O$ is 32.2 kcal/mol more exothermic than that of C_2H_4O. This difference in ΔG is similar to that in ΔE(G2MS with ZPE), 40.7 kcal/mol, for nucleophilic addition of H_2O to C_2H_4O and $C_6H_{10}O$. The release of additional ring strain in $C_6H_{10}O$ during the insertion process accounts for the large difference in the energy of reaction for the insertion process D. In summary, using ethylene oxide instead of cyclohexene oxide gives good structure but significant errors in energy of the insertion product; the insertion of cyclohexene oxide is much more exothermic than that of ethylene oxide. Note that for coordination of epoxide there was very little difference between two epoxides.

Figure 5 also shows the optimized structures of TSs for insertion processes B and D of $C_6H_{10}O$, **InsB_ts_CHO** and **InsD_tsa_CHO**. Normal-mode analysis gives a unique imaginary frequency of 334.4i cm^{-1} for **InsB_ts_CHO** and of 310.3i cm^{-1} for **InsD_tsa_CHO**. The qualitative features of the insertion TSs have not changed from C_2H_4O to $C_6H_{10}O$. The most important reaction coordinates are breaking of the O^2-C^3 bond (ring opening) and forming of the $Zn-O^2$ σ-bond, which are followed by forming of the O^1-C^3 bond (nucleophilic addition) and breaking of the $Zn-O^1$ σ-bond. In both TSs, ring opening and nucleophilic addition are taking place asynchronously. The distance between C^3 and O^1 (or C^4 and O^3) of 2.613 Å (or 2.751 Å) is far from forming a C−O single bond. The breaking bonds, O^2-C^3 of 1.866 Å at **InsB_ts_CHO** and O^4-C^4 of 1.903 Å at **InsD_tsa_CHO**, are about 30% longer than that of $C_6H_{10}O$. Comparing with O^2-C^3 of 1.965 Å at **InsB_ts** and O^4-C^4 of 2.090 Å at **InsD_tsa**, the TSs for insertion of $C_6H_{10}O$ are earlier in stage for the ring opening. This is consistent with the prediction we have made based on the thermodynamic picture of the nucleophilic addition of water. Both bond and dihedral angles of the optimized structures of **Ins(B or D)_ts_CHO** indicate that strain in the six-membered ring has been substantially released along opening of the epoxide ring. The potential and free energies of **InsB_ts_CHO**, −0.8 and 12.8 kcal/mol relative to **I** + $C_6H_{10}O$, are 18.6 and 18.1 kcal/mol lower than that of

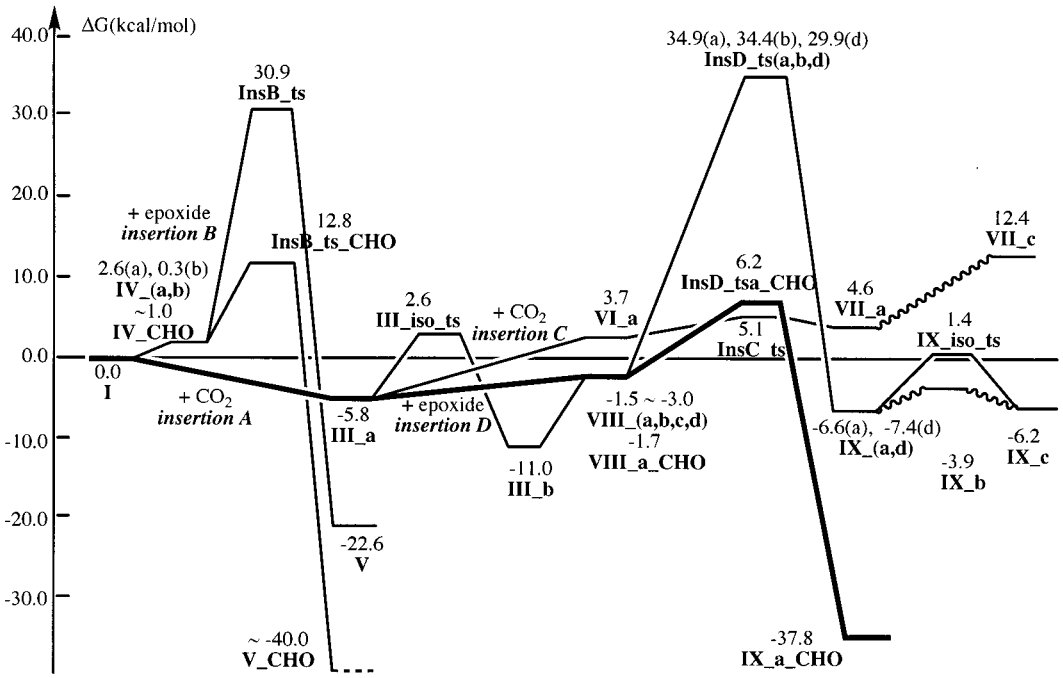

Figure 6. Gibbs free energy (298.15 K, 1 atm) profiles of insertions A−D in CO_2/ethylene oxide and cyclohexene oxide copolymerization catalyzed by (BDI)$ZnOCH_3$.

InsB_ts, respectively. Since complexation energies of C_2H_4O and $C_6H_{10}O$ are similar, the activation barrier at insertion B of $C_6H_{10}O$ should be about 12.0−13.0 kcal/mol, which is largely reduced from the C_2H_4O insertion. The potential and free energies of **InsD_tsa_CHO** are respectively −20.2 and 6.2 kcal/mol relative to **I** + CO_2 + $C_6H_{10}O$. Therefore, the activation barrier of insertion D, 9.5 kcal/mol of potential energy or 7.9 kcal/mol of free energy, is about 30 kcal/mol smaller than that of C_2H_4O. This reduction in the activation free energy is only slightly smaller than the increase in the exothermicity discussed above for the same insertion reaction.

In conclusion, $C_6H_{10}O$ instead of C_2H_4O leads to much lower activation barriers and much larger exothermicities for insertions B and D. This difference results in the large difference in the reactivity for copolymerization, as will be discussed in the next section.

F. Overall Potential and Free Energy Surfaces of Copolymerization. Before drawing overall PESs based on the ONIOM(B3LYP/BS II:PM3) results, we checked the reliability of the ONIOM energies by performing the full B3LYP/BS II single point energy calculations on the ONIOM(B3LYP/BS II:PM3) optimized structures of **I**, **VIII_a**, **InsD_tsa** and **IX_a**. As shown in Table 2, the errors of the ONIOM(B3LYP/BS II:PM3) relative energies of **VIII_a**, **InsD_tsa**, and **IX_a**, compared to those of full B3LYP/BS II are −3.0, −1.9, and +1.4 kcal/mol, respectively. Thus, the ONIOM reaction barrier and exothermicity for insertion D of C_2H_4O is overestimated by 1.1 kcal/mol and underestimated by 4.4 kcal/mol, respectively, compared to the full B3LYP values. The results indicate that for the present system the ONIOM(B3LYP/BS II:PM3) method gives nearly as reliable energies as full B3LYP/BS II.

The profiles of free energy calculated at 298.15 K (within the experimental temperature range of 20−50 °C) and 1 atm at the ONIOM(B3LYP/BS II:PM3) level for CO_2/epoxide copolymerization and competing processes are shown in Figure 6. In this Figure, the energies of **IV_CHO** and **V_CHO** are estimated on the basis of the discussion in the previous subsection.

Starting from the active catalyst, Zn−methoxy complex **I**, there are two reaction paths. One is CO_2 insertion, indicated as insertion A, and the other is epoxide insertion, indicated as insertion B in Scheme 1. As shown in Figure 6, insertion A takes place from the starting intermediate **I** without the free energy barrier and leads to Zn−carbonate complex **III_a**. For insertion B, coordination complexes have negative binding free energies and are not stable intermediates. The reaction barriers for insertion B of C_2H_4O and $C_6H_{10}O$ from the starting intermediate **I** are 30.9 and 12.8 kcal/mol, respectively. Thus, CO_2 insertion into the Zn−alkoxyl bond is kinetically much more favorable than epoxide insertion; there is no possibility for epoxide insertion to compete against the CO_2 insertion to the Zn−alkoxyl bond. Both insertions A and B are exothermic. The insertion A products, **III_a** at −5.8 kcal/mol and **III_b** at −11.0 kcal/mol, lie much higher in free energy than the insertion B products, −22.6 kcal/mol for C_2H_4O and ∼−40.0 kcal/mol for $C_6H_{10}O$. These results show a clear thermodynamic preference for insertion B over insertion A. although the kinetic preference dominates the reaction.

In summary, for insertion steps starting from complex **I**, insertion A is kinetically more favorable, although insertion B is thermodynamically more favorable. The CO_2 insertion into the Zn−alkoxyl bond is much more preferred than the epoxide insertion due to the high activation barrier required for the latter.

Starting from the CO_2 insertion product, the Zn−carbonate complex **III_a** or **III_b**, there are also two pathways. One is the second CO_2 insertion, indicated as insertion C, and the other is epoxide insertion, indicated as insertion D in Scheme 1. Coordination of the second CO_2 to Zn−carbonate is endothermic, due

to the weak σ-donating ability of CO_2 and the breaking of the chelative Zn−O interaction during coordination. The free energy barrier of insertion C from the starting intermediate **III_a** is 10.9 kcal/mol. In contrast to insertion A (CO_2 insertion into the Zn−alkoxy bond), insertion C (CO_2 insertion into the Zn−carbonate bond) is endothermic in free energy. The direct insertion product **VII_a** lies 10.4 kcal/mol above the starting intermediate in free energy, and the reverse free energy barrier for dissociation of CO_2 from the insertion product is only 0.5 kcal/mol! An isomer of **VII_a**, the more intuitive Zn−carbonate complex **VII_c**, lies 7.8 kcal/mol above **VII_a** in free energy and cannot be reached. Therefore, the insertion product is likely to dissociate quickly back to the intermediate **III_a** + CO_2, reaching equilibrium between **III_a** and **VII_a**, with **III_a** much more favored. The present results explain clearly the experimental results that polymerization of CO_2 on the Zn−alkoxyl complex **I** does not take place. While the insertion of the first CO_2 into the Zn−alkoxyl bond takes place very easily, the subsequent insertion of CO_2 into the Zn−carbonate bond is thermodynamically unfavorable; the equilibrium favors the degradation of the poly-CO_2.

On the path of insertion D, the coordination of epoxides to **III_a** or **III_b** is slightly endothermic in free energy and the starting point of the reaction is uncoordinated complex **III_a** or **III_b**. For C_2H_4O, the free energy barrier of insertion D from the intermediate **III_a** is as high as ∼35 kcal/mol. This means that the ethylene oxide insertion into the Zn−carbonate bond, like insertion B (ethylene oxide insertion into the Zn−alkoxyl bond), cannot take place. Thus, the copolymerization of ethylene oxide with CO_2 on this catalyst is out of the question. Very interestingly, however, with $C_6H_{10}O$, the energetic situation changes dramatically. The free energy barrier for insertion D of cyclohexene oxide to the intermediate **III_a** is reduced to only 12.0 kcal/mol. Now the reaction is quite feasible. The free energy of reaction from **III_a** to the product **IX_a_CHO** is as large as 32.0 kcal/mol. Thus, the reaction will be irreversible; i.e., once the insertion product is formed, it will not come back to the reactant side. Therefore, this irreversible reaction with an activation free energy of 12.0 kcal/mol can easily compete against the reversible insertion of CO_2 with an activation free energy of 10.9 kcal/mol and a reverse barrier of only 0.5 kcal/mol.

The reduction of the activation free energy, about 30 kcal/mol between the transition state **InsD_tsa** for C_2H_4O and **InsD_tsa_CHO** for $C_6H_{10}O$, is almost as large as the reduction in the free energy of reaction, about 32 kcal/mol going from **IX_a** to **IX_a_CHO**. As already discussed above, the epoxy ring is nearly completely opened at the TS and all the extra strain energy associated with the three-membered/six-membered bicyclic structure is nearly fully released already at the TS.

Briefly summarizing the insertion steps starting from Zn−carbonate complex **III**, the insertion of CO_2 has again kinetic preference, with a lower barrier than the insertion of epoxide. On the other hand, the thermodynamic preference is shown once more on the insertion of epoxide. Both preferences are qualitatively similar to the insertion reactions starting from complex **I**. However, the first CO_2 insertion into Zn−alkoxyl (insertion A) is exothermic and the CO_2 insertion into Zn−carbonate (insertion C) is endothermic and strongly reversible. The free energy barrier for insertion D of $C_6H_{10}O$ is slightly lower than insertion B of $C_6H_{10}O$. These results show that the kinetic preference for CO_2 has decreased and the thermodynamic preference for $C_6H_{10}O$ has increased from the step of insertion into the Zn−alkoxyl bond to that into the Zn−carbonate bond, respectively. Therefore, as shown in the previous paragraph, the insertion of $C_6H_{10}O$ into Zn−carbonate is globally preferred over CO_2 insertion. The competition between insertions C and D is determined by these thermodynamic factors.

Putting all the results together, the copolymerization of CO_2 and $C_6H_{10}O$ follows the path **I** → (insertion A) → **III** → **VIII_CHO** → (insertion D) **InsD_ts_CHO** → **IX_CHO**. Since insertion A occurs without a barrier, the rate-limiting step is insertion D at the ring opening of $C_6H_{10}O$, in excellent agreement with experiment results. Alternating repetition of the CO_2 insertion into the Zn−alkoxyl bond and the $C_6H_{10}O$ insertion into Zn−carbonate leads to the perfect CO_2/$C_6H_{10}O$ copolymer, i.e., polycarbonate. With a significant rate-determining barrier at the epoxide insertion into the Zn−carbonate bond, which is expected to be dependent significantly on the electronic structure, it would be interesting to control this barrier height by theoretically designing the electronic structure of the substrate (epoxide) and catalyst.

IV. Conclusions

On the basis of the above discussions, we may draw several conclusions.

1. The copolymerization reaction of CO_2/cyclohexene oxide proceeds via alternating repetition of the CO_2 insertion into the Zn−alkoxyl bond (insertion A) and the $C_6H_{10}O$ insertion into the Zn−carbonate bond (insertion D). The rate-determining step is the ring opening of $C_6H_{10}O$ during insertion D.

2. The insertion of CO_2 into either the zinc−alkoxyl (epoxide + CO_2 alternating insertion) or the zinc−carbonate (consecutive CO_2 insertion) bond has been found to be thermodynamically less favorable but is in general kinetically favored over the insertion of epoxide, due to a high barrier for the latter. However, the insertion of the CO_2 into the Zn−carbonate bond is endothermic and reversible, which prevents formation of the CO_2 polymer.

3. The insertion of epoxide into either the zinc−alkoxyl or the zinc−carbonate bond has a high barrier. This barrier is associated with a rather asynchronous transition state where the ring opening has taken place and yet the C−O bond is not formed. For instance, with ethylene oxide, the barrier for its insertion into the Zn−carbonate bond (insertion D) is too large and cannot take place.

4. Only in the case of insertion of sterically strained cyclohexene oxide into the zinc−carbonate bond, the barrier is low enough to compete against CO_2 insertion, resulting in alternating copolymerization. This lowering is driven by the release of the extra strain energy in the three-membered/six-membered bicyclic structure in cyclohexene oxide. The rate-determining step in copo-

lymerization is epoxide insertion, which can be controlled by the catalyst and the epoxide.

5. The hybrid ONIOM (B3LYP:PM3) method is found to be a good approximation to the much more expensive standard B3LYP method for the present system consisting of real catalysts and real substrates. Without the ONIOM method, the present study would not have been possible.

Acknowledgment. We are grateful to Prof. Geoffrey W. Coates, Dr. Karl Irikura, Dr. Djamaladdin G. Musaev, and Dr. Thom Vreven for many stimulating discussions. The present research is in part supported by a grant (No. CHE-9627775) from the National Science Foundation. Acknowledgment is made to the Cherry L. Emerson Center of Emory University for the use of its resources, which is in part supported by a National Science Foundation grant (No. CHE-0079627) and an IBM Shared University Research Award. Acknowledgment is also made for generous support of computing time at the National Center for Supercomputing Applications (NCSA).

OM0110843